View Article Online
View Journal

Dalton Transactions

An international journal of inorganic chemistry

Accepted Manuscript

This article can be cited before page numbers have been issued, to do this please use: A. Avallone, L. Carette, P. Estevenon, P. G. Yot, C. Hennig, E. L. Bright, R. Podor, X. F. Le Goff, P. V.B. Pinho, N. Clavier, X. Guo, C. Gueneau and N. Dacheux, *Dalton Trans.*, 2026, DOI: 10.1039/D6DT01220E.

ROYAL SOCIETY OF CHEMISTRY

rsc.li/dalton

View Article Online
DOI: 10.1039/D6DT01220E

Revisiting Synthesis of Pure chernobylite Solid Solutions for Thermal Stability Investigations

Arthur Avallone [1], Léna Carette [1], Paul Estevenon [2], Pascal G. Yot [3], Christoph Hennig [4, 5], Eleanor Lawrence Bright [4, 5], Renaud Podor [1], Xavier Le Goff [1], Pâmella V. B. Pinho [6], Nicolas Clavier [1], Xiaofeng Guo [7, 8], Christine Guéneau [6], Nicolas Dacheux [1, *]

[1] ICSM, Univ Montpellier, CNRS, CEA, ENSCM, Bagnols-sur-Cèze, France
[2] CEA, DES, ISEC, DMRC, Univ Montpellier, Marcoule, France
[3] ICGM, Univ Montpellier, CNRS, ENSCM, Montpellier, France
[4] Institute of Resource Ecology, Helmholtz Zentrum Dresden-Rossendorf (HZDR), PO Box 510119, 01314 Dresden, Germany
[5] The Rossendorf Beamline at ESRF, The European Synchrotron, CS40220, 38043 Grenoble Cedex 9, France
[6] Université Paris-Saclay, CEA, Service de recherche en Corrosion et Comportement des Matériaux, Gif-sur-Yvette, France
[7] Department of Chemistry, Washington State University, Pullman, Washington 99164, United States
[8] Alexandra Navrotsky Institute for Experimental Thermodynamics, Washington State University, Pullman, Washington 99164, United States

* Corresponding of author: nicolas.dacheux@umontpellier.fr

Abstract

A multiparametric study was developed to optimize the hydrothermal synthesis of chernobylite solid solutions ($Zr_{1-x}U_xSiO_4$), a phase first discovered in the Elephant's foot of the Chernobyl nuclear power plant following the 1986 nuclear accident. The goal was to obtain phase-pure samples for thermodynamic investigation. Optimal synthesis conditions were determined starting from uranium(IV) and zirconium(IV) chloride precursors, using a hydrothermal treatment for seven days at 250 °C with a reaction medium maintained within a pH range of 1.4 to 1.8, which minimized the formation of secondary phases Under these conditions, solid solutions of chernobylite were synthesized up to x = 0.80. However, the systematic presence of residual oxide phases in the samples required the development of a purification process involving alternating leaching steps in basic and nitric media. This process removed amorphous silica and selectively dissolved residual oxide phases, respectively. This protocol yielded pure $Zr_{1-x}U_xSiO_4$ samples over a wide range of compositions ($x \leq 0.6$). The resulting powders consisted of spherical agglomerates of approximately 300 µm in diameter, with specific surface areas ranging from 19 to 22 $m^2 \cdot g^{-1}$. Finally, the thermal stability of the chernobylite solid solutions was evaluated using heat treatments between 1000°C and 1300°C. All samples, except for those most enriched in uranium, proved to be thermally stable even at 1300°C.

Keywords

Zircon, Zirconium silicate, Uranium silicate, Hydrothermal synthesis, Sample purification, Chernobylite

View Article Online
DOI: 10.1039/D6DT01220E

1. Introduction

In the event of a severe accident in a nuclear light water reactor, loss of the core cooling system can cause a rapid rise in temperature, leading to melting of the uranium dioxide (UO_2) fuel then its interaction with surrounding materials: the zirconium alloy cladding and the steel vessel. This process results in the formation of a complex mixture of solid and liquid phases, known as “in-vessel corium”. In the case of vessel breach, the corium may flow out of the reactor vessel and interact with the concrete basement, forming “ex-vessel corium”, containing different silicate and oxide phases.[1]

Three major accidents of this type have marked the history of nuclear energy: Three Mile Island (1979), Chernobyl (1986), and Fukushima Daiichi (2011).[2] In the Chernobyl accident, the explosion of the Unit 4 reactor, followed by a fire, led to a partial meltdown of the core and the formation of the so-called "Chernobyl lava".[3,4] This lava contains chernobylite (also called chornobylite), a mixed silicate of zirconium and uranium with the formula $(Zr,U)SiO_4$, which results from a reaction between mixed oxide $(U,Zr)O_2$ and silicates coming from concrete.[5]

Zircon ($ZrSiO_4$) and coffinite ($USiO_4$), two silicate phases with high natural occurrence, belong to the orthosilicate class.[6] Both crystallize in a zircon-type tetragonal structure, in which silicon is tetra-coordinated in $[SiO_4]$ units, while zirconium (Zr) or uranium (U) occupies dodecahedral polyhedra with triangular faces.[7] This structural similarity between both silicates suggests the potential formation of a continuous solid solution $(Zr,U)SiO_4$.

Zircon has been extensively studied due to its high chemical and structural stability under extreme conditions, making it a reference material in geochronology and materials science.[8] Indeed, $ZrSiO_4$ has long been studied as a host matrix for the specific immobilization of actinides, particularly plutonium, due to its high chemical and structural stability over geological timescales. Zircon can incorporate tetravalent actinides (U^{4+}, Th^{4+}, and Pu^{4+}) through substitution at the Zr site, while retaining low solubility and high resistance to self-irradiation damage. Natural zircons enriched in uranium and thorium are natural analogues that demonstrate effective long-term retention of actinides, making them suitable candidate for sustainable storage of nuclear waste.[9–11] Conversely, coffinite is more difficult to prepare and is much less characterized as a synthetic pure phase despite its abundance in nature. It is frequently found at equilibrium with uranium oxide UO_{2+x} and is the second main uranium(IV) bearing phases after uraninite (UO_2).[12] Coffinite formation is favored by the omnipresence of dissolved silica in geological environments, corresponding to a process known as “coffinization”.[13,14] This process has been experimentally confirmed recently in tests involving the dissolution of uranium oxides in silicate solutions.[15–17]

Although zircon syntheses using both dry and wet chemistry routes appear to be fairly straightforward, obtaining phase-pure coffinite remains a long-standing challenge. In particular, zircon has actually been prepared using hydrothermal methods for over a century. Von Chrustschoff reported the first zircon synthesis under hydrothermal conditions as early as 1892.[18] Recently, Barral *et al.* conducted a multiparametric study to optimize conditions for obtaining this phase.[19] Their work revealed that zircon can be produced as a pure phase across a large pH domain (ranging from 1 $mol \cdot L^{-1}$ HNO_3 to pH = 9). However, carbonate-rich media prevent the formation of $ZrSiO_4$.[20] From a kinetic point of view, zircon formation is associated with slow kinetics, requiring hydrothermal treatment at

View Article Online
DOI: 10.1039/D0DT01220E

250°C for at least seven days. Conversely, numerous attempts to synthesize coffinite since the 1950s have emphasized the challenge of controlling synthesis conditions, particularly the U/Si ratio and pH values.[21] These variables must be kept within very narrow ranges to avoid the formation of secondary phases. The pioneering work of Fuchs and Hoekstra, followed by Mesbah *et al.*[16,21] laid the bases of hydrothermal approaches. More recently, Szenknect *et al*. proposed an optimized protocol for preparing phase-pure coffinite,[22] which involved hydrothermal synthesis under controlled conditions of pH (11.4 and then 8.7), temperature (250°C), and treatment duration (7 days).[15] Coffinite formation necessarily required a large quantity of carbonates[15], which is incompatible with zircon synthesis.[20] This is mainly due to the formation of uranium (IV) silicate complexes, which act as precursors for larger colloidal species and coffinite through aging. However, this silicate-uranium (IV) association is hindered in the presence of hydroxide ions due to the rapid precipitation of uranium (IV) tetrahydroxide. Conversely, the presence of carbonate species in the solution leads to the complexation of uranium and inhibits uranium hydroxide formation. As the coffinite samples prepared were always polyphase, a purification cycle was always applied for the selective dissolution of the secondary phases (UO_2 and SiO_2), which occurred in acidic and basic media, respectively.[23]

Hydrothermal synthesis has proven to be an advantageous route for preparing actinide silicates, $MSiO_4$ (M = Th, Pu, U).[16,24] In particular, Barral *et al.* and Estevenon *et al.* recently explored the possibility of preparing solid solutions of $Zr_{1-x}Ce_xSiO_4$ and $Zr_{1-x}U_xSiO_4$ *via* this route.[19,25] Despite the incompatible synthesis conditions between $ZrSiO_4$ and $USiO_4$, it was possible to obtain chernobylite solid solutions (up to 60 mol.% U) within phase mixtures containing oxide-type phases. However, the solid solutions prepared by Estevenon *et al.* [25] were largely polyphasic due to the high tendency of uranium to hydrolyze. Hence, optimizing the preparation of pure chernobylite samples for advanced characterization remains necessary.

Therefore, comprehensive experimental study of solid solutions between zircon and coffinite is essential for determining the solubility limits of zirconium and uranium in the phase, establishing optimal synthesis conditions, and understanding the role of the formation of these phases in severe accident scenarios and geological nuclear waste disposal. The objective of this study is to optimize the synthesis conditions for chernobylite solid solutions with (U/U+Zr) ≤ 0.8 by studying the influence of several parameters, including the pH of the reaction medium and the hydrothermal treatment duration. Second, a purification protocol is presented to eliminate traces of secondary phases, such as oxides and amorphous silica. The purified samples are then subjected to high-temperature heat treatments to investigate the impact of uranium content on the thermal stability of chernobylite solid solutions.

View Article Online
DOI: 10.1039/D6DT01220E

2. Materials and methods

Caution: Natural uranium is an alpha emitter and is considered a health hazard. Experiments involving actinides require appropriate facilities and personnel trained in the handling of radioactive materials.

2.1. Preparation of the stock solutions

All chernobylite samples were synthesized by wet chemistry route under hydrothermal conditions, based on the protocol reported by Estevenon *et al.*[25] To this end, several stock solutions were prepared. The uranium (IV) solution was obtained by dissolving uranium metal chips in concentrated hydrochloric acid, as described by Dacheux *et al.*[26]. First, the chips were successively washed with acetone, distilled water, and with a 1 mol·L^{-1} HCl solution to remove any oxide layer that may have formed on their surface. This step was essential to prevent traces of uranium (VI) ending up in the final solution. Next, the chips were dissolved in a 6 mol·L^{-1} HCl solution prepared by dilution of concentrated HCl (12 mol·L^{-1}, supplied by Sigma-Aldrich). The mixture was refluxed for several hours. The zirconium solution was obtained by dissolving anhydrous zirconium tetrachloride ($ZrCl_4$, Sigma-Aldrich, purity ≥ 99.5 %) in a 1 mol·L^{-1} HCl solution. The concentrations of the cationic solutions were determined using inductively coupled plasma optical emission spectroscopy (ICP-OES; iCAP 7000 Plus Series, Thermo Scientific), following the conditions reported in section 2.5.7. The concentrations were found to be 0.61 ± 0.02 mol·L^{-1} for the uranium solution and 0.839 ± 0.002 mol·L^{-1} for the zirconium solution. Additionally, the silicate solution was prepared by dissolving sodium metasilicate (Na_2SiO_3, Sigma-Aldrich, 307815) in distilled water. Before performing the hydrothermal treatment, the pH of the mixture was adjusted between 1.0 and 2.7 using a 8 mol·L^{-1} NaOH solution, which was prepared by dissolving solid sodium hydroxide (Sigma-Aldrich, ACS reagent, ≥ 97.0 %, pellets) in distilled water.

2.2. Hydrothermal synthesis of chernobylite

A protocol inspired by the one used for zircon was adopted to synthesize chernobylite solid solutions samples with U/(U+Zr) ≤ 0.8.[19,25] This protocol is presented in **Figure 1**. First, a mixture of the two cations (Zr and U) was prepared. Then, a volume of silicate solution was added dropwise to the mixture while stirring. This volume was considered to maintain a 5 mol.% excess of silicon in the mixture. This slight excess ensured that the cations precipitate completely while limiting the formation of large quantities of amorphous silica in the final mixture. The volumes of each solution were adjusted to set the total cation concentration ($C_U + C_{Zr}$) at 0.2 mol·L^{-1}. To maintain a constant volume of 10 mL, deionized water was added to the mixture. Next, a volume of sodium hydroxide solution (8 mol·L^{-1} NaOH) was added to the acidic starting mixture (≈ 1 mol.L^{-1} HCl) to adjust the pH of the reaction medium to the expected value (1 ≤ pH ≤ 2.7). The mixture was introduced into a Parr device (model no. 4749), which consisted of a 23 mL polytetrafluoroethylene (PTFE) insert (considering a dead volume representing one-third of the total volume), and was placed in an oven at 250°C according to the protocol described by Estevenon *et al.*[25] To limit the formation of oxide phases, the initial pH of the reaction medium was adjusted between 1.0 and 2.7, while the duration of the hydrothermal treatment (t) ranged from 1 to 21 days. The goal in optimizing this synthesis method was to produce

View Article Online
DOI: 10.1039/D6DT01220E

$Zr_{1-x}U_xSiO_4$ solid solutions with minimal secondary phases to simplify the purification process prior to in-depth physicochemical and thermodynamic characterization. It is important to note that, according to the literature, coffinite samples are often described as hydrated or hydroxylated after hydrothermal treatment, but as anhydrous after high-temperature calcination. For simplicity, the formula $Zr_{1-x}U_xSiO_4$ was adopted for the entire study, without making any assumptions about the degree of hydration or hydroxylation of the samples obtained after hydrothermal treatment and the purification step.

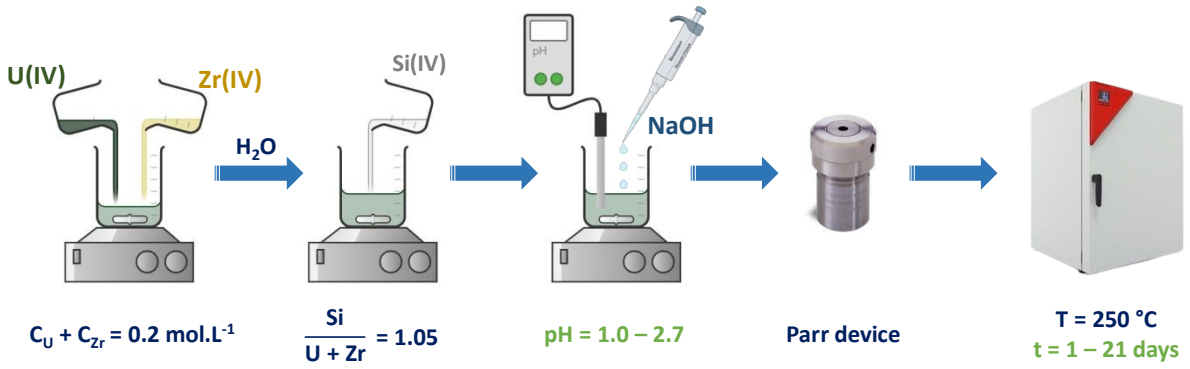

Figure 1. Experimental protocol optimized for the hydrothermal synthesis of chernobylite solid solutions, inspired from Estevenon *et al.*[25]

2.3. Purification protocol

All purification cycles were carried out using a method inspired from Clavier *et al.*[23] for $Th_{1-x}U_xSiO_4$ solid solutions and adapted by Estevenon *et al.*[25] for $Zr_{1-x}U_xSiO_4$ solid solutions. This method consisted in alternated washing with an acidic medium (HNO_3) and a basic medium (KOH) to remove oxide and amorphous silica fractions, respectively. The nitric acid solutions used in the purification cycles were prepared by diluting a concentrated HNO_3 solution (15 mol·L^{-1}, Sigma-Aldrich, ACS reagent). The basic solutions (0.01 mol·L^{-1} KOH) were obtained by dissolving solid potassium hydroxide (KOH, Sigma-Aldrich) in distilled water. The raw samples (300 mg to 1.5 g) were placed in 50 mL of the appropriate solution in 90 mL PTFE standard vials. The washing steps were carried out at 70°C for 6 to 12 hours under continuous stirring at 600 rpm. The conditions of the successive purification steps for the chernobylite samples are summarized in **Table 1**.

Table 1. Experimental conditions considered for the purification of chernobylite solid solutions samples $Zr_{1-x}U_xSiO_4$ (temperature: 70°C; stirring: 600 rpm).

Initial U mole fraction (x value)	1st step KOH – 12h	2nd step HNO_3 – 6h	3rd step KOH – 12h
0 – 0.2	0.01 mol·L^{-1}	0.50 mol·L^{-1}	0.01 mol·L^{-1}
0.3 – 0.5	0.01 mol·L^{-1}	0.25 mol·L^{-1}	0.01 mol·L^{-1}
0.6 – 0.8	0.01 mol·L^{-1}	0.10 mol·L^{-1}	0.01 mol·L^{-1}

View Article Online
DOI: 10.1039/D6DT01220E

2.4. Study of the thermal stability

Chernobylite solid solution samples were then subjected to heat treatments to evaluate the thermal stability of the silicate phase and its ability to retain uranium in the solid solution. The experimental procedure consisted of calcining the powders in a Carbolite tubular furnace (STF 14/180, 1400°C) equipped with a quartz tube under a reducing atmosphere (Ar – 4% H_2) to prevent the uranium (IV) from oxidation to uranium (VI) throughout the heat treatment. For each composition, the same powder was successively heated for 6 h at 1000°C, 1100°C, 1200°C and 1300°C, with characterization carried out after each thermal treatment. Five compositions (x = 0.05, 0.20, 0.30, 0.50, and 0.60) were studied.

2.5. Characterization of chernobylite samples (raw, purified, annealed)

All prepared samples, whether raw from synthesis, purified, or heated at high temperatures, were systematically analyzed using various conventional characterization techniques.

2.5.1. Powder X-Ray Diffraction (PXRD). X-ray diffraction characterization was performed on two different devices. Most of the samples were analyzed using high-resolution X-ray diffraction (HR-XRD) on the Rossendorf Beamline (ROBL) at the European Synchrotron Radiation Facility (ESRF). The powders were placed in 0.3-mm-diameter glass capillaries and inserted into Kapton tubes, providing the double confinement barrier required for handling of radioactive samples. Then, they were mounted on metal supports, which allowed for acquisition in rotation conditions. X-ray diffractograms were recorded at an energy of 16,200 eV (λ = 0.7654 Å) over an angular range of 0° to 60° (2θ), with a a Dectris Eiger CdTe 500k detector. The distance sample-detector, geometrical parameters of the detector and wavelength were calibrated using NIST standard LaB_6. All the two dimensional recorded images were integrated using pyFAI software, giving an effective step size of 0.0012°.[27] Some other samples were analyzed using a Bruker D8 Advance diffractometer with Cu $K\alpha_{1,2}$ radiation (λ = 1.5418 Å) over an angular range of 5 to 95° (2θ), with a step size of 0.02°. The radioactive samples were confined in an air-tight polymethylmethacrylate (PMMA) specimen holder with a X-ray transparent dome (Bruker A100B33 sample holder). All PXRD patterns have been normalized to enable comparison. The PXRD patterns obtained for all the compositions were first indexed using DICVOL06 [28] and unit-cell parameters were determined using LeBail procedure included in JANA 2006 suite [29] by refining the PXRD patterns in the 2-theta range 5-66°, using Pseudo-Voigt peak profile and manual background correction. To compare the different PXRD patterns, a systematic conversion to wave vector was performed. Regarding polyphase samples, the diffractograms were subsequently refined using the Rietveld method with the JANA 2006 software.[29] This method allowed for the determination of the mass fractions of each phase in polyphasic samples. During the refinement process, several instrumental and structural parameters were adjusted, including the 2θ shift, lattice parameters, scale factor, and profile parameters. However, the occupancies of metallic elements were adjusted using the unit cell parameters determined for each composition and fixed during the refinement.

2.5.2. Environmental Scanning Electron Microscopy (ESEM). Micrographs were recorded using environmental scanning electron microscopy (ESEM, Thermo Scientific Quattro S) in secondary

View Article Online
DOI: 10.1039/D6DT01220E

electron (SE) and backscattered electron (BSE) modes with acceleration voltages ranging from 5 to 15 kV. EDS mappings were performed on the same device using a Bruker X-Flash 6–100 detector with a working distance of 10.4 mm and an acceleration voltage of 15 kV. The obtained X-ray maps were converted to QMap for the quantitative estimation of the chemical composition.

2.5.3 Transmission Electronic Microscopy (TEM). Transmission electron microscope (TEM), Scanning transmission electron microscopy (STEM), and energy-dispersive X-ray spectroscopy (EDS) mapping with line scanning analysis were carried out using a FEG JEOL 2200FS microscope equipped with a field emission gun operating at 200 kV. EDS measurements in STEM mode were carried out using an Oxford Instruments X-Max N 100 TLE 100 mm² windowless silicon drift detector (SDD) and a focused electron probe with a diameter of approximately 0.7 nm. Samples were prepared by dispersing a small amount of powder in ethanol. A drop of the resulting suspension was deposited onto a copper grid coated with a holey carbon film and allowed to dry prior to analysis

2.5.4. Raman Spectroscopy. Spectra were recorded in backscattering geometry configuration, with 1800 gr·mm^{-1} holographic grating and 200 µm hole width on a Horiba Soleil confocal Raman microscope, using a 532 nm excitation wavelength. The laser spot size focused on the sample was ≈ 1 µm, with a × 50 long working distance (11 mm) objective, at a power kept lower than 0.51 mW in order to avoid any heating or structural sample damage. At this power, neither shift in position nor intensity modification of any band induced by laser heating was observed. The acquisition time was between 100 and 500 s. Between 2 and 6 scans were performed and averaged to obtain the best signal to noise ratio.

2.5.5. ThermoGravimetric Analysis (TGA). A SETSYS Evolution TG/DT analyzer was used for thermogravimetric analysis (TGA) to estimate the water content of the samples and to study the thermal stability of chernobylite solid solution $Zr_{1-x}U_xSiO_4$. Measurements were performed between room temperature and 1000°C under reducing conditions (Ar – 4% H_2) with a heating and cooling rate of 10°C·min^{-1}.

2.5.6. Determination of the specific surface area by BET method. The specific surface area of the powders was determined by nitrogen adsorption/desorption at – 196°C using the Brunauer–Emmett–Teller (BET) method with a Micromeritics Tristar 3020 device. Prior to analysis, approximately 200–300 mg of powder underwent a degassing step at 100°C for 4 hours. The obtained specific surface area values were also used to estimate the average particle sizes, assuming spherical shapes and using the calculated theoretical density from the unit cell volumes according to **Eq. 1.**

$$d_{\text{particle}} = \frac{k}{\rho_{\text{theo}} \times S_{\text{BET}}} \quad (1)$$

Where the shape factor *k* equals 6, assuming spherical particles, ρ_{theo} is the theoretical density, and S_{BET} is the specific surface area determined by the BET method. The theoretical density was calculated using **Eq. 2**.

View Article Online
DOI: 10.1039/D6DT01220E

$$\rho_{\text{theo}} = \frac{M \times Z}{N_a \times a^3} \times \frac{1}{\rho_w} \quad (2)$$

Where M is the molar mass of the mixed oxide (g·mol^{-1}), Z is the number of formula units per unit cell (Z = 4 for zircon), N_A is Avogadro's number (mol^{-1}), a is the unit cell parameter (cm), determined from Rietveld refinement of the XRD patterns and ρ_w corresponds to the water density (g·cm^{-3}).

2.5.7. Determination of the precipitation and purification yields by ICP-OES and UV spectrometry. In order to estimate the precipitation and purification yields, the concentrations of uranium and zirconium in the initial solutions were measured by ICP-OES (iCAP 7000 Plus Series, Thermo Scientific). Calibration was performed using certified standard solutions (PlasmaCAL, SCP Science, 1000 mg·L^{-1} in 0.2 mol·L^{-1} HNO_3). The selected wavelengths for uranium were λ = 263.553, 367.007, 385.958, and 393.203 nm; those for zirconium were λ = 257.139, 327.305, 339.198, 343.823, and 349.621 nm. The limit of detection (LoD) was 0.01 mg·L^{-1} for both elements.

Silicon concentrations were determined using a method based on forming yellow heteropolyacid complexes from molybdate and silicate ions (Spectroquant Test 1.01813.0001, Sigma-Aldrich). The absorbance of these complexes was monitored at λ = 410 nm using a Shimadzu UV-3600 spectrophotometer in PMMA cuvettes. Measurements were taken over a wavelength range of 300 to 500 nanometers, with a step size of 0.2 nanometers. This method allowed us to determine the concentration of silicate ions (or colloidal silica) in solution from 0.25 µg·L^{-1} to 1 g·L^{-1}.

2.5.8. Fourier Transform InfraRed Spectroscopy (FTIR). Fourier transform infrared (FTIR) spectra were recorded using a PerkinElmer Spectrum 100 FTIR spectrometer within the 415 – 4000 cm^{-1} range. Powdered samples were placed directly on the surface of an attenuated total reflectance (ATR) crystal without prior preparation. The spectra acquired under these operating conditions had a resolution of less than 2 cm^{-1}. One hundred scans were performed for each sample to average out instrumental error.

View Article Online
DOI: 10.1039/D6DT01220E

3. Results and discussion

3.1. Optimization of synthesis conditions for $Zr_{0.5}U_{0.5}SiO_4$

The synthesis method, inspired by the one of zircon, was found to be incompatible with the coffinite synthesis reported in the literature. Therefore, we expected to optimize first the synthesis protocol of $Zr_{0.5}U_{0.5}SiO_4$ solid solution. Preliminary results obtained using this composition showed that, despite the initial mixture having a high uranium content, this silicate phase could be prepared under the conditions recently reported by Estevenon *et al.* [25] However, as expected, the resulting product was not single phase and associated with the formation of a large amount of oxide. To reduce the quantity of secondary phases within the prepared samples, we optimized the synthesis conditions of $Zr_{0.5}U_{0.5}SiO_4$. by studying the influence of treatment duration and pH of the reaction medium.

3.1.1. Impact of hydrothermal treatment duration

The first step consisted of varying the duration of hydrothermal treatment from 1 day to 3 weeks at pH = 1.6 and T = 250°C. **Figure 2** shows the PXRD patterns obtained for all the considered durations. According to these data, the zircon-type structure phase is present in all the prepared samples. However, as expected from the results reported by Estevenon *et al.*,[25] a second oxide phase was also observed. Refinement of the lattice parameters (see **Table 2,** an example of a Rietveld refinement pattern is presented in **Figure SI.1**) suggested that the duration of the hydrothermal treatment had little effect on the composition of the silicate phase. In fact, the lattice volume was found to be 282.37(1) Å³ after one day and 282.48(1) Å³ after 21 days, highlighting only a slight variation (see **Figure SI.2**). Under these experimental conditions, the silicate phase appeared stable. Based on the unit cell volumes reported in the literature for zircon and coffinite[16,30], the uranium incorporation rate within this phase remained almost constant, with an average value estimated at approximately 48.6 $\pm$ 2.2 mol.%, close to the expected value. Therefore, it appeared that the precipitation of the two cations occurred simultaneously and quantitatively. Although the duration of the hydrothermal treatment had little impact on the composition of the chernobylite phase, it significantly affected the relative quantity between the zircon-type ($I4_1/amd$) and fluorite-type ($Fm\bar{3}m$) structures formed. While the oxide percentage in the mixture was close to 10 $\pm$ 2 wt.% after one day, it decreased down to 5 $\pm$ 2 wt.% after 7 to 14 days, becoming nearly undetectable (< 2 wt.%) after 21 days of hydrothermal treatment. Analysis of unit-cell parameters indicated an apparent uranium content of about 86.7 ± 1.3 mol.% in the oxide phase, calculated with the assumption that an oxygen-stoichiometric U–Zr mixed oxide was obtained (i.e. with O/(U+Zr) = 2.00). It is worth noting that some amounts of UO_2 were also formed in the samples prepared after 7 and 14 days. However, to prevent the oxidation of uranium (IV) during hydrothermal treatment, a duration of 7 days was considered as the best compromise and was adopted for all subsequent experiments. It is also important to note that two silicate phases with similar compositions were obtained for the sample prepared after 3 days of hydrothermal treatment. This phenomenon, only observed for this treatment duration, is unlikely to be related to kinetic or thermochemical effects. Rather, it could be related to small heterogeneity of the starting mixture during the synthesis of this sample (e.g. due to less efficient stirring step). Further tests will be conducted to precise the origin of the second silicate phase in this sample.

View Article Online
DOI: 10.1039/D6DT01220E

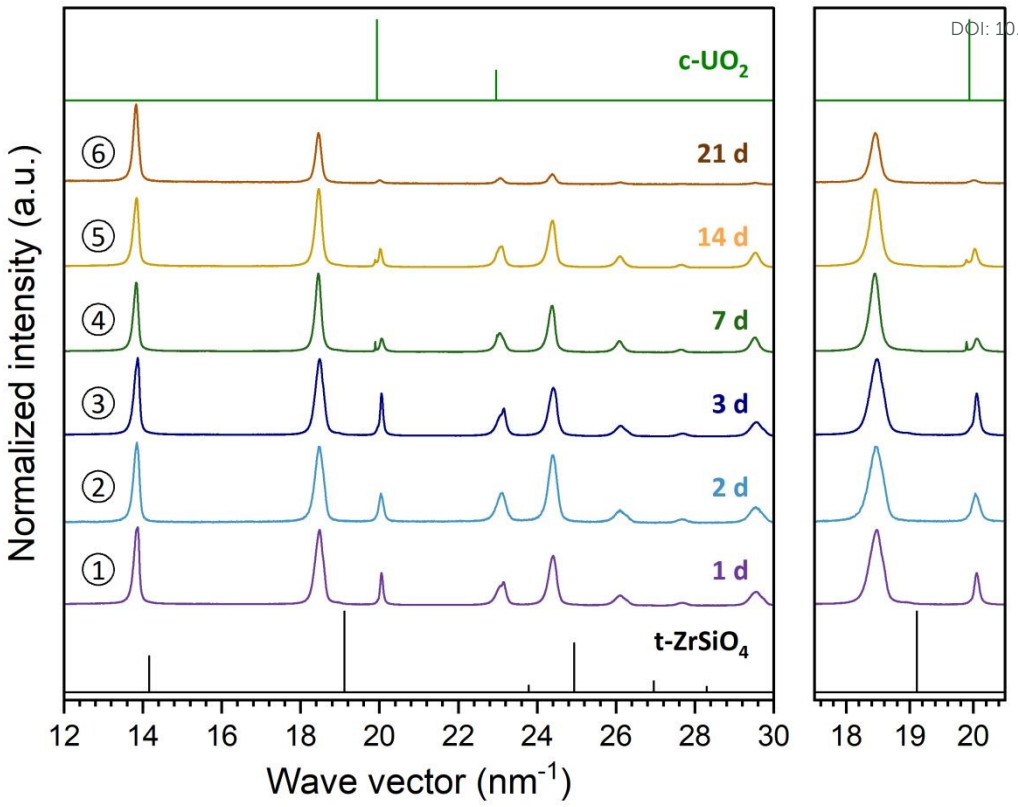

Figure 2. PXRD patterns of raw solid solution samples of chernobylite containing 50 mol.% uranium, synthesized by the hydrothermal route (T = 250°C, $pH_{initial}$ = 1.6, $C_U + C_{Zr}$ = 0.2 mol·L^{-1}) for (1) 1 day, (2) 2 days, (3) 3 days, (4) 7 days, (5) 14 days, and (6) 21 days. Samples (2) and (6) were analyzed using laboratory XRD device (λ = 1.5418 Å) whereas samples (1), (3), (4) and (5) were analyzed at the ROBL beamline at ESRF (λ = 0.7654 Å). Reference data for tetragonal zircon (t-$ZrSiO_4$)and cubic UO_2 (c-UO_2) are taken from [30] and [31], respectively.

View Article Online
DOI: 10.1039/D6DT01220E

Table 2. Unit cell parameters, uranium mole fractions and quantities of each phase determined in the samples prepared under hydrothermal conditions for various durations (1-21 days).

t (days)	Phase *	Unit cell parameters			U mole fraction #	Phase quantity (wt.%)
		a (Å)	*c* (Å)	*V* (Å^3)		
1	Si	6.8041(1)	6.0993(1)	282.37(1)	0.48	90 ± 2
	Ox	5.42329(6)	--	159.51(1)	0.86	10 ± 2
2	Si	6.8028(4)	6.0983(4)	282.22(4)	0.48	92 ± 2
	Ox	5.4231(4)	--	159.49(4)	0.86	8 ± 2
3	Si-1	6.8139(1)	6.1082(1)	283.60(1)	0.51	50 ± 2
	Si-2	6.7741(1)	6.0879(1)	279.36(1)	0.42	41 ± 2
	Ox	5.42244(6)	--	159.43(1)	0.86	9 ± 2
7	Si	6.8156(1)	6.1090(1)	283.78(1)	0.51	95 ± 2
	Ox-1	5.46997(3)	--	163.665(3)	1.00	1 ± 1
	Ox-2	5.4237(1)	--	159.54(1)	0.86	4 ± 1
14	Si	6.8049(1)	6.1000(1)	282.48(1)	0.48	95 ± 2
	Ox-1	5.4653(1)	--	163.24(1)	0.99	1 ± 1
	Ox-2	5.4283(1)	--	159.95(1)	0.88	4 ± 1
21	Si	6.8050(1)	6.1001(1)	282.48(1)	0.48	98 ± 2
	Ox	5.4337(1)	--	160.44(1)	0.89	2 ± 1

* Si : zircon-type structure, Ox : fluorite-type structure

U mole fraction determined with the assumption that all uranium was tetravalent in the structure

3.1.2. Impact of the pH of the initial reaction medium

As it is well documented in the literature, uranium (IV) exhibits a strong tendency to hydrolyze. This hydrolysis leads to the formation of poorly crystallized hydroxides and amorphous gels, which can evolve into oxides. Preliminary results obtained for pH ≥ 3 showed the formation of this gel within the reaction mixtures, which systematically resulted in oxide as the dominant phase (see **Figure SI.3** for pH = 2.7). Furthermore, the presence of this gel caused heterogeneity problems within the initial mixture due to insufficient stirring. Thus, the effect of pH was studied over the range 1.0 – 2.7 (the range in which no gel was formed). The results obtained by PXRD, varying the pH value of the starting mixtures, are shown in **Figure 3.** Results obtained from Rietveld analysis (*i.e.*, unit cell parameters and volume, U mole fraction in each phase as well as phase quantity) are reported in **Table 3** (an example of a Rietveld refinement pattern is presented in **Figure SI.4**). Moreover, **Figure 4** shows the variation in unit-cell volume as a function of the pH of the reaction medium.

View Article Online
DOI: 10.1039/D6DT01220E

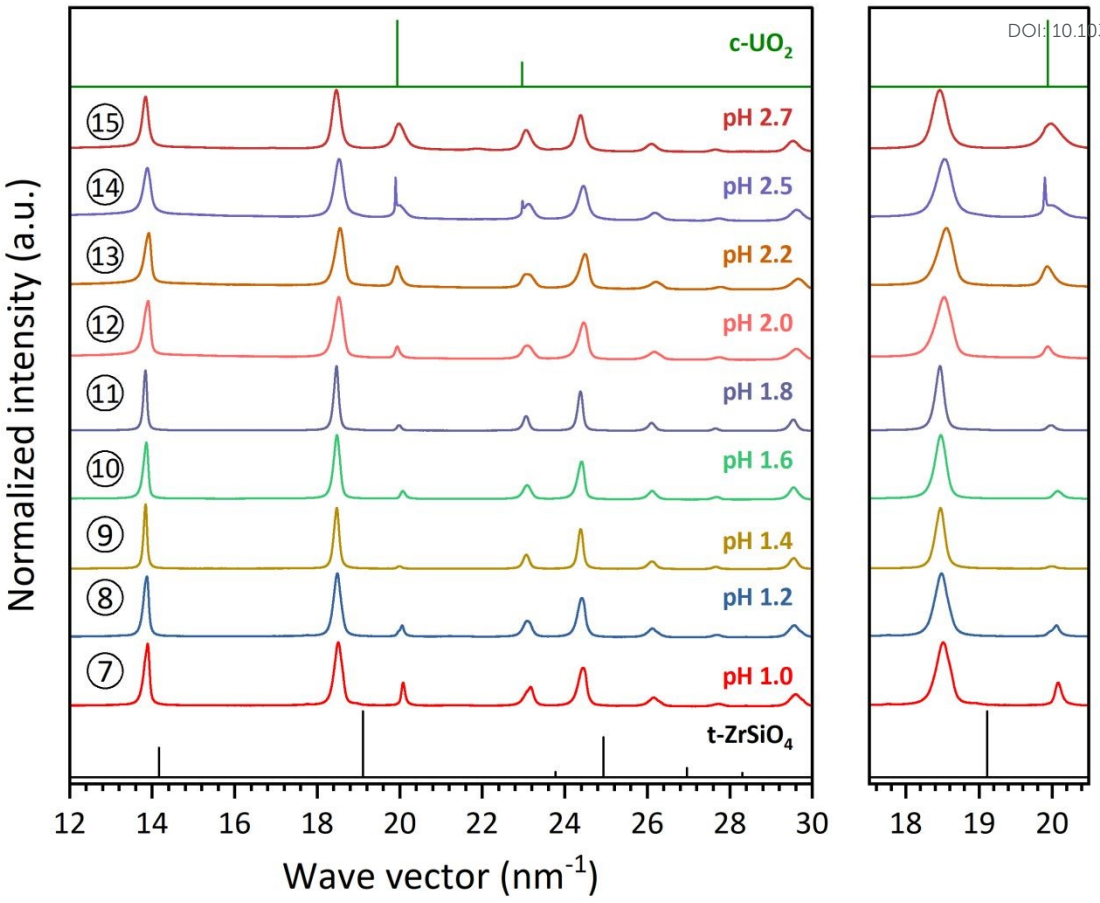

Figure 3. PXRD patterns of raw chernobylite solid solution samples containing 50 mol.% uranium, synthesized by the hydrothermal route (T = 250°C, t = 7 days, $C_U + C_{Zr}$ = 0.2 mol·L^{-1}) for initials pH (7) 1.0, (8) 1.2, (9) 1.4, (10) 1.6, (11) 1.8, (12) 2.0, (13) 2.2, (14) 2.5 and (15) 2.7. All the samples were analyzed at the ROBL beamline at ESRF (λ = 0.7654 Å). Reference data for tetragonal zircon (t-$ZrSiO_4$) and cubic UO_2 (c-UO_2) are taken from [30] and [31], respectively.

In **Figure 3**, there is clearly an optimal pH range for reducing the oxide amount. Indeed, between pH = 1.4 and pH = 1.8, the oxide content appeared to be minimal. Quantification of the two phases by Rietveld analysis yielded a silicate phase content of 99 ± 2 wt.% and an oxide phase content of 1 ± 1 wt.% at pH = 1.4. At pH = 1.6, these values became 97 ± 2 wt.% and 3 ± 1 wt.%, for silicate and oxide phases, respectively. Within this range, the average uranium content reached 50.2 ± 0.3 mol.% in the silicate phase, determined by Rietveld refinement (**Table 3**). This composition was consistent with what would be expected based on the initial cation mixture. Under these conditions, zirconium and uranium (IV) appeared to precipitate almost quantitatively in the pH range between 1.2 and 1.8 (with precipitation yields greater than 87 % based on the mass balance). For lower pH values (*i.e.*, for pH ≤ 1.2), the oxide content increased slightly (5 ± 1 wt.% at pH = 1.0), whereas a decrease in the uranium content in the silicate phase (47 mol.% at pH = 1.0) was observed. Conversely, for higher pH values (i.e. for pH ≥ 2.2), the oxide amount in the samples increased strongly, reaching 10 ± 2 wt.% and 16 ± 2 wt.% at pH = 2.2 and pH = 2.7, respectively. At the same time, the uranium content within the silicate phase decreased to 43 mol.% at pH = 2.2.

View Article Online
DOI: 10.1039/D6DT01220E

Furthermore, the analysis of the PXRD patterns revealed that two types of oxide phases often coexisted as secondary phases. The first had a lattice parameter close to that of stoichiometric or slightly hyper-stoichiometric UO_{2+x}, suggesting a predominantly uranium enriched phase with a composition close to $UO_{2.00}$ and limited incorporation of zirconium. The second phase, on the other hand, had a significantly lower unit cell volume than UO_2. Two hypotheses can be considered in this case: a more pronounced oxidation of uranium dioxide UO_{2+x}, which would lead to the contraction of the unit cell parameter due to the decrease in cationic radius ($^{VIII}r_{U^{5+}}$ = 0.89 Å compared to $^{VIII}r_{U^{4+}}$ = 1.00 Å); or a partial incorporation of zirconium ($^{VIII}r_{Zr^{4+}}$ = 0.84 Å) in substitution of uranium (IV) into the fluorite-type structure.

Table 3. Unit cell parameters, uranium mole fractions and quantities of each phase determined in the samples prepared under hydrothermal conditions for various starting pH values (1.0 – 2.7).

pH	Phase *	Unit cell parameters			U mole fraction #	Phase quantity (wt.%)
		a (Å)	*c* (Å)	*V* (Å^3)		
1.0	Si	6.7975(1)	6.0981(1)	281.77(1)	0.47	95 ± 2
	Ox	5.41907(4)	--	159.138(3)	0.85	5 ± 1
1.2	Si	6.8070(1)	6.1035(1)	282.81(1)	0.49	96 ± 2
	Ox-1	5.4500(1)	--	161.88(1)	0.94	1 ± 1
	Ox-2	5.4278(1)	--	159.91(1)	0.87	3 ± 1
1.4	Si	6.8102(1)	6.1035(1)	283.23(1)	0.50	99 ± 2
	Ox	5.4477(1)	--	161.67(1)	0.94	1 ± 1
1.6	Si	6.8115(1)	6.1068(1)	283.34(5)	0.50	97 ± 2
	Ox	5.4227(1)	--	159.46(1)	0.86	3 ± 1
1.8	Si	6.8122(1)	6.1082(1)	283.46(1)	0.51	98 ± 2
	Ox	5.4491(1)	--	161.80(1)	0.94	2 ± 1
2.0	Si	6.7958(1)	6.0940(1)	281.44(1)	0.46	96 ± 2
	Ox	5.4582(7)	--	162.62(6)	0.97	4 ± 1
2.2	Si	6.7821(1)	6.0845(1)	279.88(1)	0.43	90 ± 2
	Ox	5.4548(1)	--	162.31(1)	0.96	10 ± 2
2.5	Si	6.7917(1)	6.0946(1)	281.13(1)	0.45	91 ± 2
	Ox-1	5.47054(3)	--	163.716(2)	1.00	2 ± 1
	Ox-2	5.4412(1)	--	161.10(1)	0.92	7 ± 2
2.7	Si	6.8141(1)	6.1087(1)	283.63(1)	0.51	84 ± 2
	Ox	5.4463(1)	--	161.55(1)	0.93	16 ± 2

* Si : zircon-type structure, Ox : fluorite-type structure

U mole fraction determined with the assumption that all uranium was tetravalent in the structure

Figure 4 shows the variation of the lattice volume of the zircon-type phase as a function of the initial pH of the reactive media. Between pH 1.0 and 1.4, the lattice volume increased with pH and approached the expected composition, in line with the decrease in the amount of oxide formed

View Article Online
DOI: 10.1039/D0DT01220E

(**Table 3**). An optimal range was observed between pH 1.4 and 1.8, where the amount of oxide was minimal and the composition of the solid solution was closest to the target composition. Between pH 1.8 and 2.2, the lattice volume decreased as pH increased, suggesting the gradual formation of a secondary oxide phase, at the expense of uranium incorporation into the silicate, in line with Rietveld refinement results. Finally, between pH 2.2 and 2.7, the increase in lattice volume could reflect hydration of the solid solutions and swelling of the crystal lattice, a phenomenon expected under more alkaline conditions, which would be consistent with the results already observed for hydrothermally synthesized $ZrSiO_4$.[19] **Figures SI.5** and **Table SI.6** present the results of the thermogravimetric analysis (TGA) performed on the solid solutions of chernobylite synthesized at pH = 1.6. For all compositions studied, the measured degree of hydration corresponded to 0.3–0.5 water molecules per formula unit. These low values indicate that the synthesis conditions at pH = 1.6 result in low hydration of the samples.

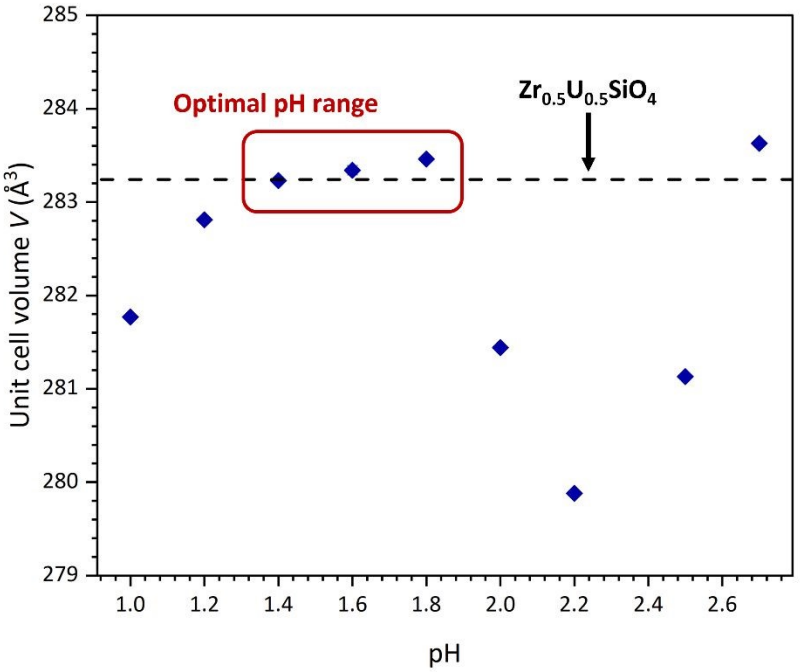

Figure 4. Variation of the unit cell volume of the chernobylite solid solution $Zr_{0.5}U_{0.5}SiO_4$ versus the pH in the starting mixture.

3.2. Synthesis of other compositions of $Zr_{1-x}U_xSiO_4$ solid solutions

Based on the results obtained for $Zr_{0.5}U_{0.5}SiO_4$, the optimal conditions for preparing chernobylite solid solution were determined to be an initial pH of 1.6 in the reaction mixture and a 7-day hydrothermal treatment. These conditions, known to favor the formation of zircon but not coffinite [16], were applied to all other compositions, *i.e.* from x = 0 to x = 0.80. The PXRD diagrams are shown in **Figure 5**, and the results of refinement are shown in **Table 4 (**an example of a Rietveld refinement pattern is presented in **Figure SI.7**). They all show the systematic formation of the silicate phase. This contrasts with previous syntheses carried out at pH = 3, where the formation of silicate was no longer observed for the highest uranium-rich compositions (i.e., x ≥ 0.70), as reported by Estevenon *et al.*[25]

View Article Online
DOI: 10.1039/D5DT01220E

Even for x > 0.6, the results differed from previous findings. The silicate phase remained present in the mixture but seemed to be destabilized by increasing the formation of a secondary oxide phase.

Up to x = 0.6, the gradual shift of the silicate-associated peaks toward smaller wave vectors (see insert in **Figure 5**) indicates the progressive increase in uranium incorporation into the silicate structure. This is consistent with the difference between U(IV) and Zr in terms of ionic radius. However, for x ≥ 0.65, a significant fraction of uranium was no longer incorporated into the silicate structure and instead formed one or more oxide-based phases. For example, at x = 0.65, these oxide phases accounted for 28 ± 5 wt.%, compared with 10 ± 1 wt.% for x = 0.60. Their proportion increased progressively with uranium content, from 4 ± 1 wt.% at x = 0.50 to 53 ± 5 wt.% at x = 0.80. These oxide phases were also strongly enriched in uranium. Thus, we noted the systematic presence of several secondary oxides, the total quantity of which increased with the overall uranium content in the system.

Under optimal conditions for preparing chernobylite solid solution samples, the maximum amount of uranium that was found to be incorporated was 60 mol.%. Beyond this value, the amount of oxide in the samples increased. This increase of oxide resulted in less uranium being incorporated into the silicate phase, leading to the decrease in the unit cell volume. As instance, uranium content decreased from 60 mol.% at x = 0.60 down to 56 mol.% at x = 0.7. This development could have suggested the possibility of a structural limit on the incorporation of uranium into the zircon structure. However, coffinite $USiO_4$ cannot be obtained under these conditions. Therefore, we cannot rule out competition between the kinetics of silicate phase formation and that of uranium hydroxide precipitation as the pH of the solution increases. For uranium enriched compounds, saturation with respect to uranium (IV) hydroxide (pKs = 54.5 ± 1.0) [32] could have been reached, which could have led to its rapid precipitation and its subsequent aging to the oxide phase. Moreover, some small traces of minor oxides, most likely zirconia, were detected in compositions with the lowest uranium contents (*i.e.* 0, 3, and 10 mol.%). Furthermore, the silicate peaks showed pronounced asymmetry in the x = 0.10–0.20 composition range compared with the other samples, which may reflect a modification in the uranium incorporation mechanism. This asymmetry required the refinement to be performed with two silicate phases. Additional experiments combining HR-PXRD, EXAFS, and HERFD are currently in progress to clarify this specific behavior.

View Article Online
DOI: 10.1039/D6DT01220E

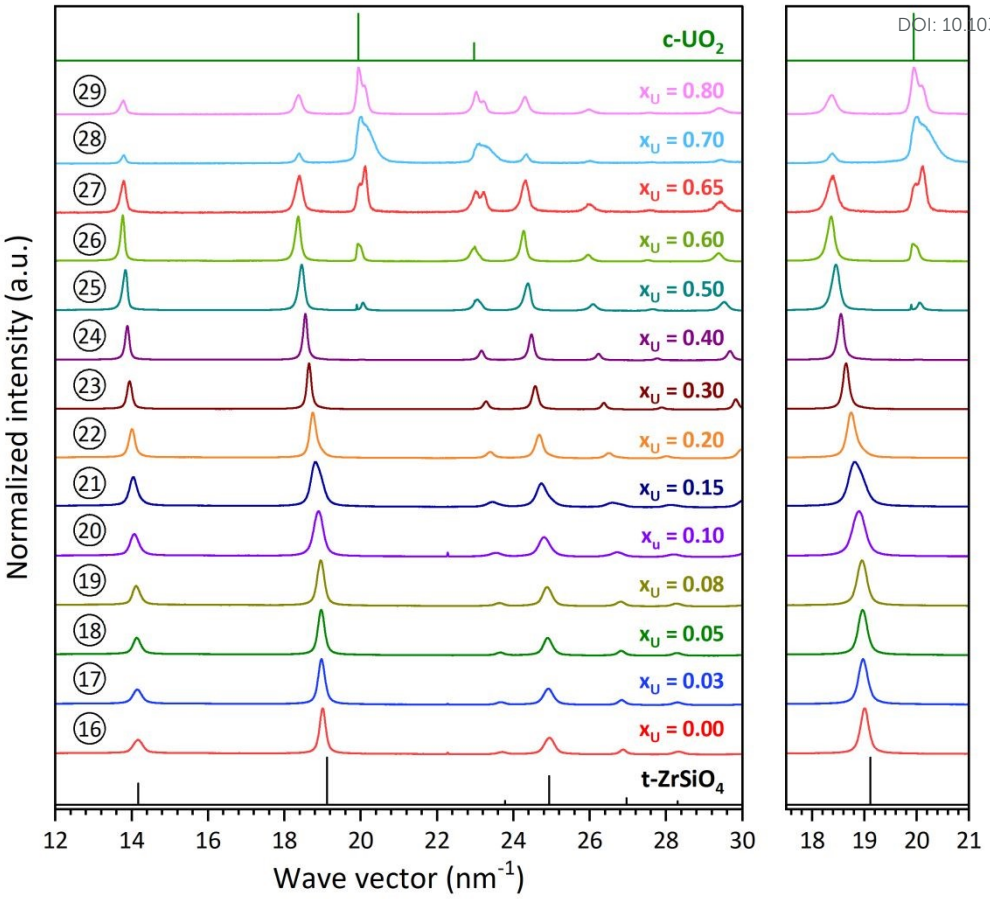

Figure 5. PXRD patterns of raw chernobylite solid solution samples synthesized by the hydrothermal route (T = 250°C, t = 7 days, $C_U + C_{Zr}$ = 0.2 mol·L^{-1} and $pH_{initial}$ = 1.6) with an initial target composition of (16) 0.00, (17) 0.03, (18) 0.05, (19) 0.08, (20) 0.10, (21) 0.15, (22) 0.20, (23) 0.30, (24) 0.40, (25) 0.50, (26) 0.60, (27) 0.65, (28) 0.70 and (29) 0.80 mol.% U. Samples (27), (28) and (29) were analyzed using laboratory XRD device (λ = 1.5418 Å) whereas samples (16) to (26) were analyzed at the ROBL beamline at ESRF (λ = 0.7654 Å). Reference data for tetragonal zircon (t-$ZrSiO_4$) and cubic UO_2 (c-UO_2) are taken from [30] and [31], respectively.

View Article Online
DOI: 10.1039/D6DT01220E

Table 4. Unit cell parameters, uranium mole fractions and quantities of each phase determined in the samples prepared under hydrothermal conditions (T = 250°C, t = 7 days, $C_U + C_{Zr}$ = 0.2 mol·L^{-1} and $pH_{initial}$ = 1.6) for various chemical compositions of starting mixtures.

$\frac{U}{U+Zr}$	Phase*	Unit cell parameters			U mole fraction #	Phase quantity (wt.%)
		a (Å)	*c* (Å)	*V* (Å^3)		
0.00	Si	6.6134(1)	5.9809(1)	261.59(1)	--	100§
0.03	Si	6.6208(1)	5.9858(1)	262.38(1)	0.04	100§
0.05	Si	6.6204(1)	5.9866(1)	262.34(1)	0.04	100§
0.08	Si	6.6224(1)	5.9873(1)	262.58(1)	0.05	100§
0.10	Si-1	6.6340(3)	5.9965(1)	263.91(1)	0.08	100§
	Si-2	6.6813(1)	6.108(1)	272.7(1)	0.27	
0.15	Si-1	6.6420(1)	5.9984(1)	264.63(1)	0.08	100§
	Si-2	6.6988(1)	6.0379(1)	270.94(1)	0.23	
0.20	Si-1	6.6506(2)	6.0180(2)	266.17(2)	0.13	100§
	Si-2	6.70684(4)	6.04168(6)	271.765(4)	0.25	
0.30	Si	6.7402(1)	6.0623(1)	275.41(1)	0.33	100§
0.40	Si	6.77822(6)	6.08536(6)	279.588(5)	0.42	100§
0.50	Si	6.8161(1)	6.1091(1)	283.83(1)	0.51	96 ± 2
	Ox-1	5.47001(5)	--	163.669(8)	1.00	1 ± 1
	Ox-2	5.4237(1)	--	159.5(1)	0.86	3 ± 1
0.60	Si	6.8501(1)	6.1342(1)	287.84(1)	0.60	90 ± 2
	Ox-1	5.4612(1)	--	162.88(1)	0.98	5 ± 1
	Ox-2	5.4390(1)	--	160.90(1)	0.91	5 ± 1
0.65	Si	6.8438(4)	6.1259(4)	286.92(4)	0.58	72 ± 5
	Ox-1	5.4575(3)	--	162.55(3)	0.97	10 ± 5
	Ox-2	5.4162(3)	--	158.89(2)	0.84	18 ± 5
0.70	Si	6.8398(5)	6.1147(6)	286.06(5)	0.56	20 ± 5
	Ox-1	5.4508(3)	--	161.95(3)	0.95	20 ± 5
	Ox-2	5.3937(3)	--	156.91(3)	0.77	60 ± 5
0.80	Si	6.8481(3)	6.1263(3)	287.30(3)	0.59	47 ± 5
	Ox-1	5.4606(2)	--	162.83(2)	0.98	28 ± 5
	Ox-2	5.4172(2)	--	158.97(2)	0.84	25 ± 5

* Si : zircon-type structure, Ox : fluorite-type structure

U mole fraction determined with the assumption that all uranium was tetravalent in the structure

§ Oxide content below the detection limit

Figure 6.a shows the scanning transmission electron microscopy micrograph of the $Zr_{0.35}U_{0.65}SiO_4$ solid solution (sample 27), revealing several distinct morphologies. At the same time, SEM observations were also performed on the $Zr_{0.4}U_{0.6}SiO_4$ sample prepared at pH = 2.7 showing more oxide content as secondary phase (see **Figure SI.8.a**).

View Article Online
DOI: 10.1039/D6DT01220E

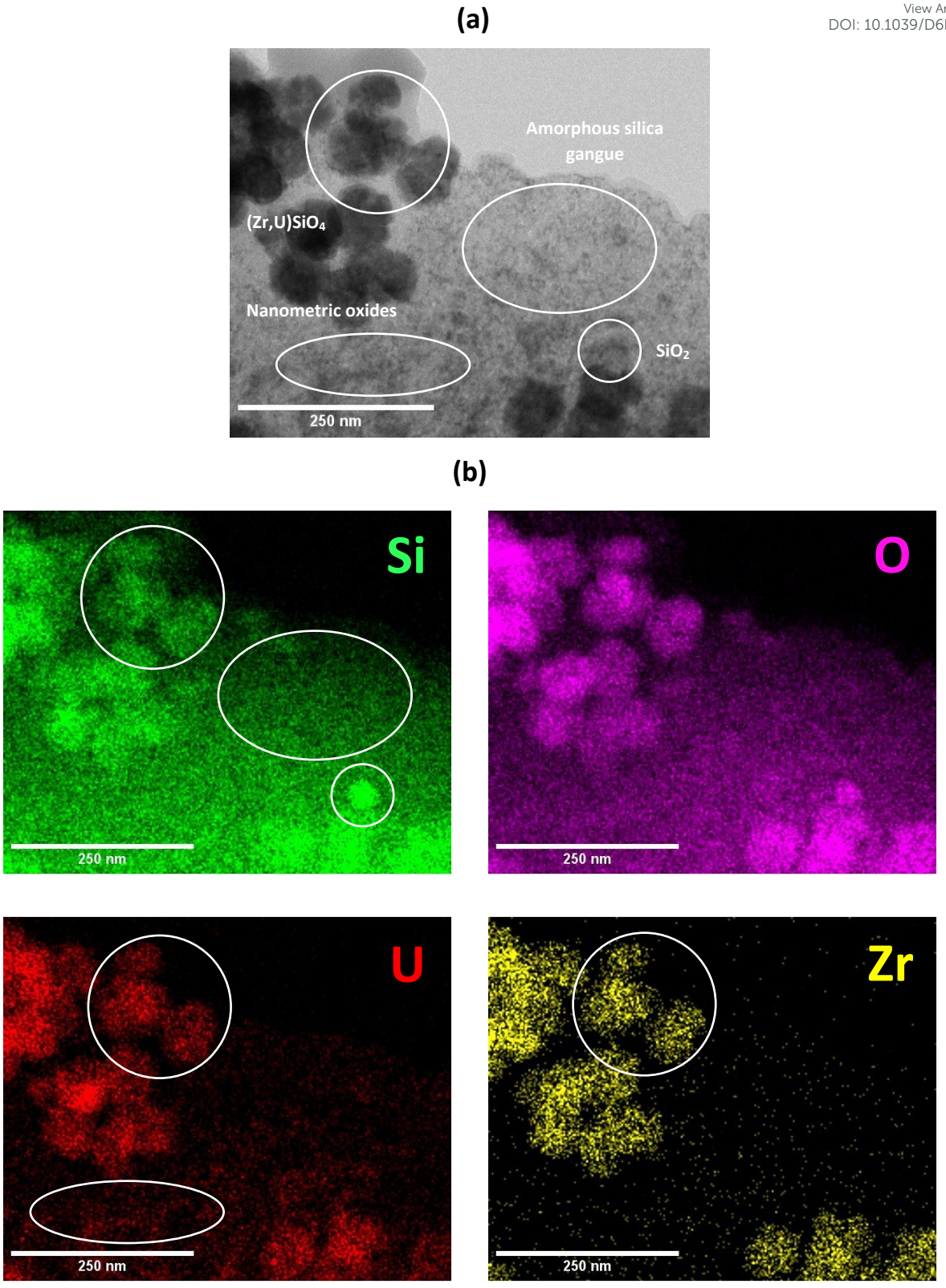

Figure 6. Transmission Electron Microscopy study of raw $Zr_{0.35}U_{0.65}SiO_4$ solid solution. (a) Bright-field STEM (BF-STEM) micrograph and (b) STEM-EDS analysis with the corresponding elemental maps of Si, O, Ti, and Zr, showing the elemental distribution.

View Article Online
DOI: 10.1039/D6DT01220E

In **Figure 6.a**, the first morphology corresponds to spherical particles measuring about 70 nm in diameter. These particles are characteristic of chernobylite solid solutions, as described in our previous work. These particles correspond to aggregates of elongated crystallites of approximately 10 nm in length. They are associated to apparent porosity. The second morphology consists of nanometric particles that are characteristic of a secondary phase, specifically an oxide phase. STEM observations and X-EDS mapping of the same sample (**Figure 6.b**) confirm the presence of a nanometric secondary phase enriched in uranium and depleted in zirconium and silicon. In contrast, the spherical particles exhibit uniform cation and silicate distribution. Visible amorphous silica is also present and forms a matrix that coats the solid solutions of chernobylite, as well as the nanometric oxide particles. Few traces of crystallized silica are also present. Despite optimizing the preparation of the chernobylite solid solutions, the samples with the highest uranium contents were polyphasic. For this reason, a purification procedure was developed for samples derived from hydrothermal synthesis to remove such traces of mixed oxides and amorphous silica.

View Article Online
DOI: 10.1039/D6DT01220E

3.3. Purification and characterization of the purified products

According to previous studies, despite optimizing the synthesis conditions in terms of hydrothermal treatment duration and of the pH of the starting reaction medium, the samples with high uranium content (*i.e.* U/U+Zr > 0.5) still contained residual oxides as secondary phases.[25] These oxides were identified as either hyper-stoichiometric uranium oxide or uranium-zirconium oxide solid solutions. However, EDS analyses of the polyphase samples (**Figure 6.b**) revealed a secondary phase enriched in uranium. Therefore, it was more likely to be stoichiometric uranium oxide rather than a uranium-zirconium oxide solid solution. The secondary oxide phase consisting mainly of stoichiometric uranium oxide ($UO_{2.00}$) also made the purification process more efficient. In fact, incorporating zirconium into the fluorite-type structure could enhance the chemical durability of the materials (zirconia being resistant to dissolution), as already reported for thorium in $U_{1-x}Th_xO_2$ solid solutions .[33] Conversely, uranium-rich oxides are less resistant to dissolution, which should also improve the purification efficiency.[34] Therefore, a purification process was implemented to purify the samples. This process was inspired by the work carried out on uranothorite solid solutions ($Th_{1-x}U_xSiO_4$).[23] It was based on the selective dissolution of residual amorphous silica in a basic medium and oxide phase in an acidic medium. The composition of the media was adapted to that of the samples (see **Table 1**). To improve the purity of the samples, a second leaching step in basic medium was added to end the purification cycle (**Figure 7**). The first stage of leaching in basic medium was intended to remove most of the amorphous silica. This stage was essential to make the oxide particles accessible during the second stage of leaching in an acidic medium. Reversing the leaching steps (*i.e.* acid then basic washing) led to much less effective purification of the sample. Nitric acid was used to promote dissolution of the oxide through oxidation of uranium (IV) present in uranium oxides. The final step in basic medium eliminated any residual traces of amorphous silica. A temperature of 70°C was chosen to preserve the silicate phases and increase the dissolution kinetics of the secondary phases. **Figure 7** illustrates the different steps of the methodology used. Compared to preliminary tests, the combination of stirring and heating improved the efficiency of the purification process while preserving the silicate phase during prolonged contact with the acid solution. To optimize the purification process, we first used a uranium-enriched chernobylite solid solution ($Zr_{0.4}U_{0.6}SiO_4$) containing a significant amount of oxide, as secondary phase. The protocol was then applied to all the prepared solid solutions.

Table 5 shows the concentrations of U, Zr, and Si measured in the supernatants after each of the 3 purification steps. As previously mentioned, the first leaching step in a basic medium removed amorphous silica. The measured silicon (Si) concentrations in the supernatants confirmed the increase in silica content in the samples as the targeted uranium composition increases. These values ranged from 4.5×10^{-5} mole for x = 0.50 to 2.8×10^{-4} mole for x = 0.70. Additionally, no traces of uranium or zirconium were observed in the supernatants during this first leaching step. Measurements taken during the second leaching step in nitric acid solution showed the presence of uranium, which is characteristic of the removal of the secondary oxide phase. The amount of uranium increased with the target U content in the solid solutions of chernobylite, which is consistent with the higher mass fractions of secondary oxide phases in these samples. However, starting at x = 0.65, zirconium was

View Article Online
DOI: 10.1039/D5DT01220E

present in the supernatant, which can be explained by the presence of mixed-oxide secondary phases $U_{1-x}Zr_xO_2$. Thus, zirconium was carried along with the uranium during dissolution. During this second washing step, only small amounts of silicon were also observed in solution, indicating a slight alteration of the silicate phase during purification in nitric acid. Finally, silicon concentration measurements during the final washing step in a basic medium highlighted the importance of this step. Indeed, few amounts of residual silica remained mixed with the samples after treatment with nitric acid.

Table 5. Amounts of U, Zr and Si measured during the basic/acid/basic purification steps of chernobylite solid solution.

Purification step		Uranium molar fraction in chernobylite				
		0.50	**0.60**	**0.65**	**0.70**	**0.80**
		Quantity (mol)				
1st	U	< LoD*	< LoD	< LoD	< LoD	< LoD
	Zr	< LoD	< LoD	< LoD	< LoD	< LoD
	Si	4.5×10^{-5} (≈1 %)	8.5×10^{-5} (≈2 %)	1.9×10^{-4} (≈3.5 %)	2.8×10^{-4} (≈5 %)	1.8×10^{-4} (≈3.5 %)
2nd	U	$(1.9 \pm 0.2) \times 10^{-6}$ (≈0.1 %)	$(6.0 \pm 0.2) \times 10^{-5}$ (≈2 %)	$(1.2 \pm 0.1) \times 10^{-4}$ (≈4 %)	$(3.5 \pm 0.1) \times 10^{-4}$ (≈10 %)	$(3.0 \pm 0.1) \times 10^{-4}$ (≈8 %)
	Zr	< LoD	< LoD	$(2.4 \pm 0.2) \times 10^{-6}$ (≈0.1 %)	$(4.9 \pm 0.4) \times 10^{-5}$ (≈3 %)	$(1.2 \pm 0.1) \times 10^{-5}$ (≈1 %)
	Si	1.3×10^{-5} (≈0.3 %)	4.6×10^{-5} (≈1 %)	5.9×10^{-5} (≈1 %)	1.5×10^{-5} (≈1.5 %)	5.6×10^{-5} (≈1 %)
3rd	U	< LoD	< LoD	< LoD	< LoD	< LoD
	Zr	< LoD	< LoD	< LoD	< LoD	< LoD
	Si	4.4×10^{-5} (≈1 %)	3.4×10^{-5} (≈0.5 %)	< LoD	1.2×10^{-4} (≈2 %)	2.0×10^{-5} (≈0.5 %)

* LoD: Limit of Detection

View Article Online
DOI: 10.1039/D6DT01220E

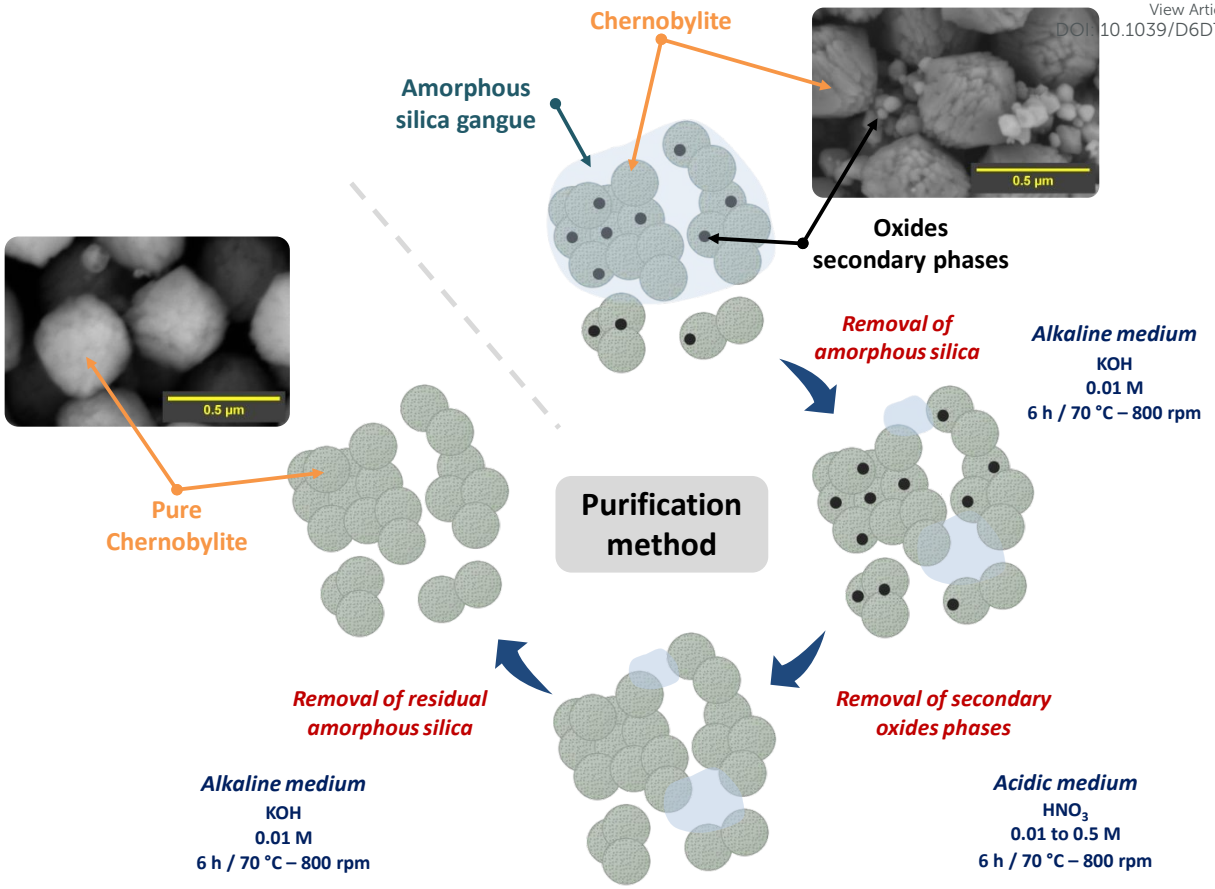

Figure 7. Description of the methodology for the selective dissolution purification of chernobylite solid solutions.

The PXRD patterns of the samples obtained after purification are shown in **Figure 8**. First, all secondary oxide phases present in the raw powders were removed during the purification cycle, regardless of their initial quantity. The complete disappearance of PXRD reflections associated with uranium oxides or mixed uranium-zirconium oxide solid solutions confirmed the high efficiency of the nitric acid-based selective dissolution protocol, which is particularly suited to low resistance to dissolution of uranium enriched oxides. Second, the silicate phase appeared to remain unaltered at the end of the purification process. No significant changes were observed in the position or shape of the PXRD reflections characteristic of the zircon structure, indicating that the purification conditions, particularly the alternation of basic and acidic media, did not compromise the integrity of the $Zr_{1-x}U_xSiO_4$ solid solution.

The results reported in **Table 6**, comparing unit cell volumes before and after purification (an example of a Rietveld refinement pattern is presented in **Figure SI.9**), confirmed the complete removal of oxide phase for all compositions studied (*i.e.* up to $x \leq 0.60$). The values calculated for the unit cell volume variations ($\Delta V/V$) indicated only minor changes in the silicate phase composition. For instance, the evaluated composition of the solid solution $Zr_{0.6}U_{0.4}SiO_4$ changed slightly from x = 0.42 (before) to x = 0.41 (after purification), whereas that of $Zr_{0.5}U_{0.5}SiO_4$ was changed from x = 0.51 (before) to x = 0.50 (after purification). Such small variations (lower than 2.4 mol.% on the relative uranium content) remained within the uncertainty associated with the refinement methods and confirmed that the

View Article Online
DOI: 10.1039/D0DT01220E

purification procedure did not affect the integrity of the main desired phase. However, due to the successive washing steps of the samples, small amounts of powder are lost, making it impossible to determine an accurate dissolution yield.

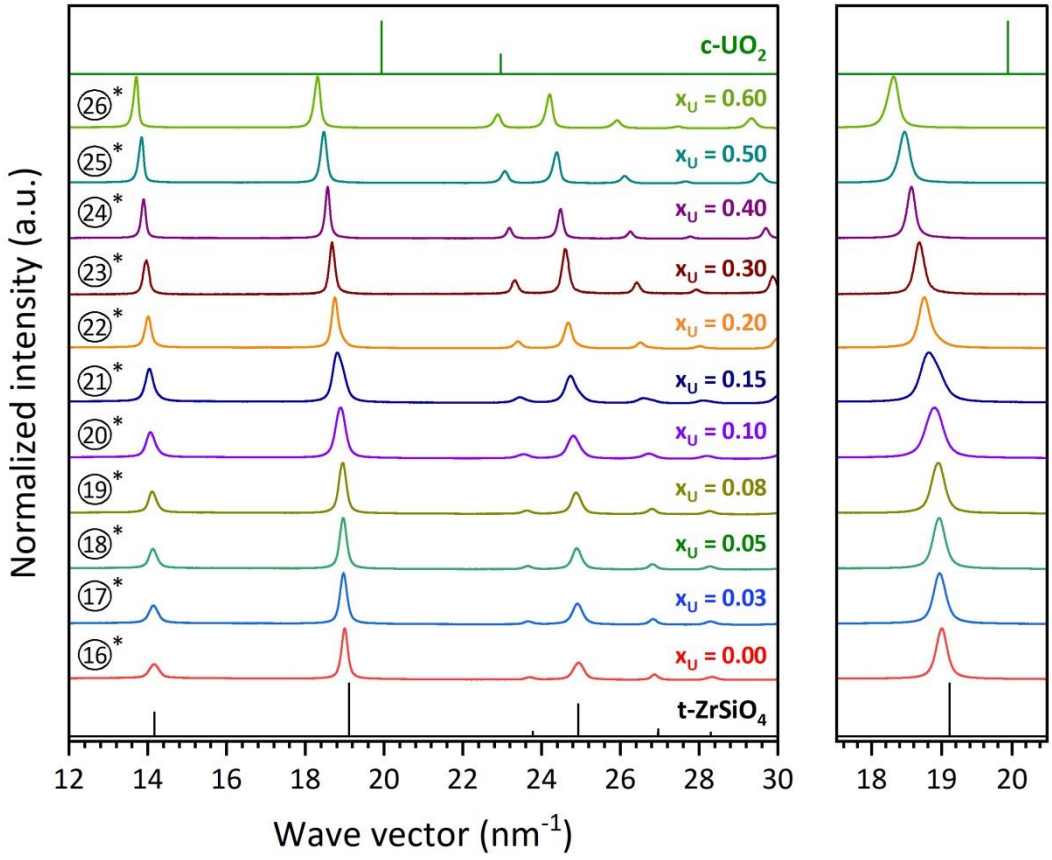

Figure 8. PXRD patterns of purified chernobylite solid solution samples synthesized by the hydrothermal route (T = 250°C, t = 7 days, $C_U + C_{Zr}$ = 0.2 mol·L^{-1} and $pH_{initial}$ = 1.6) with an initial target composition of (16) 0.00, (17) 0.03, (18) 0.05, (19) 0.08, (20) 0.10, (21) 0.15, (22) 0.20, (23) 0.30, (24) 0.40, (25) 0.50, (26) 0.60 mol.% uranium. Asterisks (*) indicate that samples were successively purified in basic and acidic media. Samples (23)* was analyzed using laboratory XRD device (λ = 1.5418 Å) whereas the other samples were analyzed at the ROBL beamline at ESRF (λ = 0.7654 Å). Reference data for tetragonal zircon (t-$ZrSiO_4$) and cubic UO_2 (c-UO_2) are taken from [30] and [31], respectively.

View Article Online
DOI: 10.1039/D6DT01220E

Table 6. Unit cell parameters, uranium mole fractions and quantities of each phase determined in the samples prepared after applying the purification protocol to the various chernobylite solid solution samples.

$\frac{U}{U+Zr}$	Phase *	Unit cell parameters of purified samples			U mole fraction #	$\frac{\Delta V}{V}$ (%) §
		a (Å)	*c* (Å)	*V* (Å³)		
0.00	Si	6.6139(1)	5.9808(1)	261.62(1)	--	+ 0.01
0.03	Si	6.6212(1)	5.9858(1)	262.42(1)	0.04	+ 0.01
0.05	Si	6.62085(5)	5.98652(5)	262.423(5)	0.04	+ 0.03
0.08	Si	6.6230(1)	5.9877(1)	262.65(1)	0.05	+ 0.03
0.10	Si-1	6.6325(1)	5.9964(1)	263.78(1)	0.07	− 0.04
	Si-2	6.7028(3)	6.1328(6)	275.53(3)	0.33	+ 0.01
0.15	Si-1	6.6368(1)	5.9881(2)	263.76(1)	0.07	− 0.33
	Si-2	6.6919(1)	6.0289(1)	269.96(1)	0.21	− 0.36
0.20	Si-1	6.6458(2)	6.0219(2)	265.97(2)	0.12	− 0.08
	Si-2	6.70327(3)	6.04115(4)	271.452(3)	0.24	− 0.12
0.30	Si	6.7305(3)	6.0573(3)	274.39(3)	0.31	− 0.37
0.40	Si	6.77124(5)	6.08373(5)	278.937(5)	0.41	− 0.23
0.50	Si	6.8097(1)	6.1092(1)	283.23(1)	0.50	− 0.21
0.60	Si	6.8443(1)	6.1355(1)	287.42(1)	0.59	− 0.15
0.65	Si	6.8339(4)	6.1243(4)	286.01(4)	0.56	− 0.01

* Si : zircon-type structure, Ox : fluorite-type structure

U mole fraction determined with the assumption that all uranium was tetravalent in the structure

§ $\frac{\Delta V}{V} = \frac{V_{purified} - V_{raw}}{V_{raw}}$

To study the nature of the obtained chernobylite solid solution, the unit cell volume of all raw and purified samples was plotted versus the expected uranium content (**Figure 9**). It clearly showed that all the data followed Retger's law (plotted as dash lines between the pure $ZrSiO_4$ and $USiO_4$ end-members) up to $Zr_{0.4}U_{0.6}SiO_4$. The lattice volume of $Zr_{1-x}U_xSiO_4$ samples increased linearly with uranium content. This reflected the substitution of Zr^{4+} by the larger U^{4+} ion within the structure. As previously mentioned, the purification step did not significantly alter the composition of the silicate phase, resulting in minor variations in unit cell volumes between the raw and purified samples. Moreover, for $0.10 \leq x \leq 0.20$, two silicate phases with a zircon-type structure coexisted. The main phase corresponds to the phase with the smallest unit cell volume at x = 0.10 and the largest at x = 0.150 and x = 0.20. This could underline a difference in the mechanism of uranium incorporation within the zircon structure. For higher uranium contents (typically between x = 0.30 and x = 0.60), the structural parameters of the chernobylite solid solution appeared to behave ideally. Beyond x = 0.60, a plateau was observed, leading to a unit cell volume of around 287 Å³, which corresponds to an effective uranium content of 0.58. This value is significantly higher than that observed in natural zircon specimens (x = 0.12) and samples prepared by dry chemistry routes (x = 0.05).[35–37] This demonstrates

View Article Online
DOI: 10.1039/D0DT01220E

the interest of preparing such solid solutions by hydrothermal treatment, as previously mentioned for other silicate phases.[16,19,38] It could also indicate a structural or thermodynamic limit to uranium (IV) incorporation within zircon structure. The thermodynamic study of chernobylite solid solution is now being conducted to check this point.

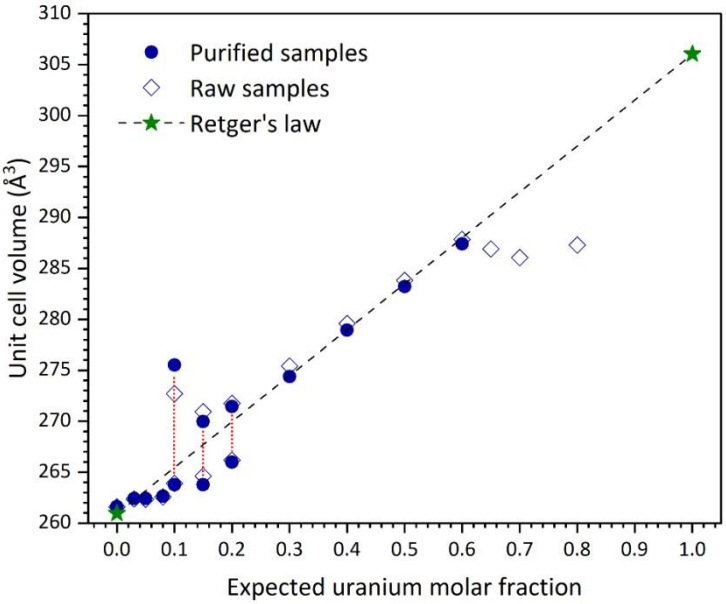

Figure 9. Variation of the unit cell volume as a function of expected uranium incorporation rate of raw (◇) and purified (●) chernobylite solid solution prepared by hydrothermal treatment (T = 250°C, t = 7 days, $C_U + C_{Zr}$ = 0.2 mol·L^{-1} and $pH_{initial}$ = 1.6). Retger's law references (★) for $ZrSiO_4$ and $USiO_4$ are taken from [30] and [39], respectively.

Figures 10.a and **Figure 10.c** show the Raman spectra of raw and purified solid solutions of chernobylite containing 65 mol.% uranium, respectively. The spectra exhibited the characteristic bands of the internal modes of the SiO_4 group. The symmetric stretching bands, labeled as ν_1, are located in the 920–980 cm^{-1} range. The symmetric bending mode, labeled as ν_2, is observed between 420 and 440 cm^{-1}. However, the antisymmetric stretching bands (ν_3), located in the 990-1040 cm^{-1} range, remained difficult to distinguish as their low intensity caused them to be partially masked by the more intense band attributed to ν_1. The antisymmetric mode, ν_4, expected around 600 cm^{-1}, was also observed. Additionally, the internal modes of the zircon structure, which are located below 400 cm^{-1}, were also observed. Apart from these bands, a signal of variable intensity appeared around 700 cm^{-1}. It was previously reported by Clavier *et al.* and associated with the optical emission of U(IV) in a zircon-type matrix when excited by a 532 nm laser. Additional vibration bands, characteristic of the fluorite-type structure of UO_2 or $U_{1-x}Zr_xO_2$ oxides, were also present in the Raman spectra of raw compound (**Figure 10.a**). Indeed, the vibrations bands corresponding to the T_{2g} and 2LO modes were observed in the 400–450 cm^{-1} and 1100-1200 cm^{-1} domains, respectively. On the other hand, these vibrational bands were absent in the Raman spectra of the purified samples (**Figure 10.c**), indicating the efficient removal of secondary oxide phases during purification. The vibrational band observed around 800 cm^{-1} can be attributed to a uranyl-type contribution; however, it could also result from the material's surface oxidizing. This oxidation may be caused by exposure to air during handling or by the laser beam

View Article Online
DOI: 10.1039/D5DT01220E

during Raman analysis. The disappearance of this band after purification, without heating treatment, suggests that it may be a secondary phase of the UO_{2+x} type.

On the other hand, **Figures 10.b** and **Figure 10.d** show the FTIR spectra of raw and purified solid solutions of chernobylite containing 65 mol.% uranium, respectively. Both spectra exhibit the characteristic bands of $Zr_{1-x}U_xSiO_4$: symmetric (ν_1) and antisymmetric (ν_3) stretching modes at 830 cm^{-1} and 975 cm^{-1}, respectively, and symmetric (ν_2) and antisymmetric (ν_4) bending modes at 430 cm^{-1} and 580 cm^{-1}, respectively. These results in good agreement with previously reported results. [25] Furthermore, **Figures 10.b** also clearly shows the presence of amorphous SiO_2 in the raw sample which can be identified with its characteristic antisymmetric bending mode at 1100 cm^{-1}. The symmetric bending mode of SiO_2 (which exhibits lower intensity than the antisymmetric mode) is hidden behind the band ν_1 of $Zr_{1-x}U_xSiO_4$. The disappearance of the SiO_2 bands between **Figures 10.b** and **Figure 10.d** confirms the removal of silica thanks to the purification procedure. In addition, both the raw and purified samples show a broad band around 3500 cm^{-1}, assigned to the O–H stretching vibration, corresponding to the presence of water molecules. This hydration is not surprising since literature reports the surface hydroxylation of samples prepared under hydrothermal conditions. This hydration/hydroxylation is typically removed through high-temperature calcination. [25]

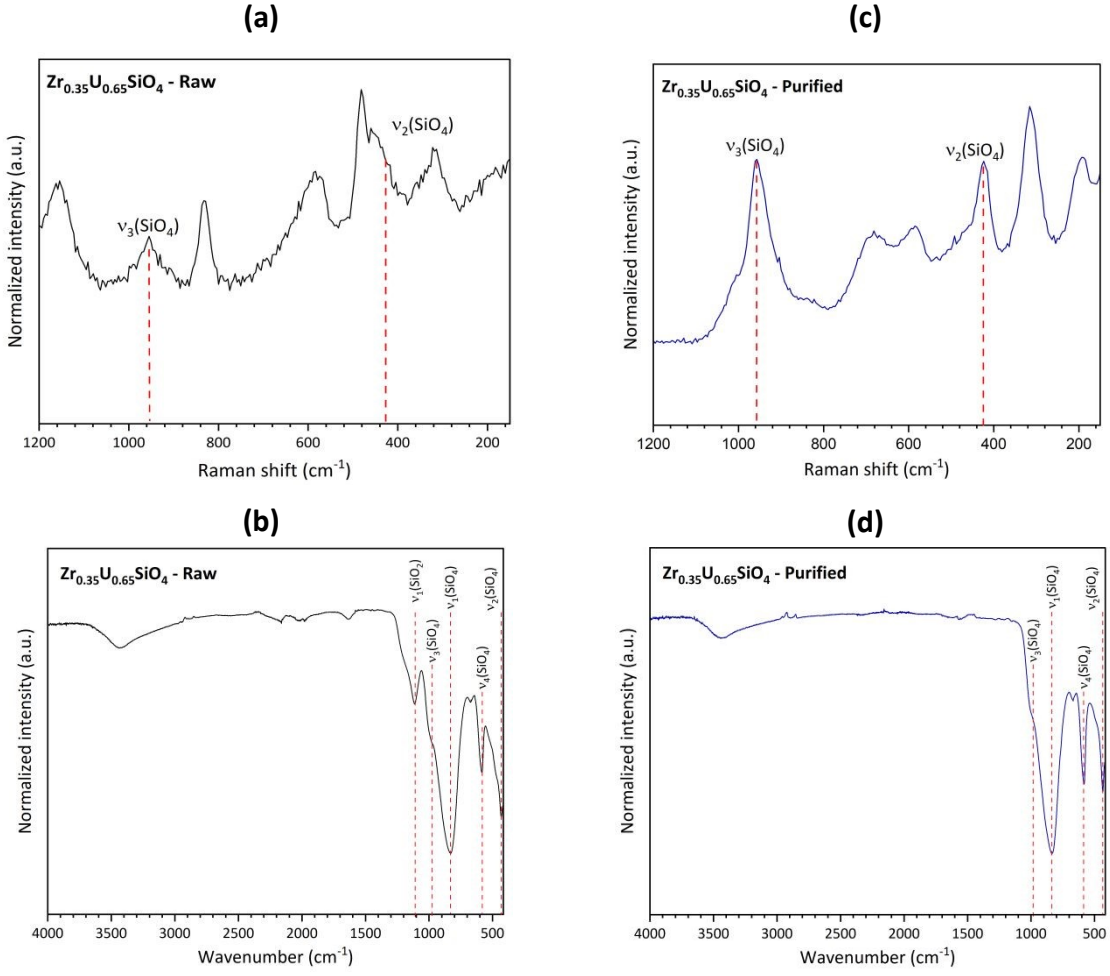

Figure 10. Raman (a,c) and FTIR (b,d) spectra of $Zr_{0.35}U_{0.65}SiO_4$ solid solution before (a, b) and after (c, d) purification procedure.

View Article Online
DOI: 10.1039/D5DT01220E

Figure 11.a shows the micrograph recorded by Transmission Electronic Microscopy of sample at the end of the purification step. It revealed that the nanometric particles associated with the oxide phase, which were initially observed in the initial sample, fully disappeared after purification. Additionally, no increase in porosity was observed in the samples following purification. These results clearly confirmed the strong efficiency of the purification protocol. Meanwhile, the chernobylite solid solution samples retained their initial morphology (spherical agglomerates of elongated crystallites, of approximately 30 nm in diameter). This suggests that they were not altered at all during the purification cycle. These results confirmed those obtained by PXRD, which showed that the chemical composition of the chernobylite solid solution samples was only slightly modified after purification. **Figure SI.10** shows a nano-diffraction pattern with the diffraction spots observed, derived from the Fourier transform of the diffracted signal. It evidenced that the chernobylite solid solution consists of aggregates composed of single-crystal assemblies. **Figure 11.b** shows a high-resolution transmission electron microscopy (TEM) image. The image reveals ordered crystal lattices, confirming the sample's crystallinity. This crystalline structure extended all the way to the edges of the single crystal, indicating that the entire sample was crystalline. Furthermore, two families of (hkl) planes can be distinguished, corresponding to atomic stacks oriented in different directions. Analysis of the (hkl) interplanar distances revealed two close values: approximately 0.47 and 0.46 nm. In this sample, these distances were attributed to two (101) and (011) crystallographic planes. The angle measured between these two planes was found to 123.2°, in good agreement with the expected value (123.7°) calculated using the refined lattice parameters of this solid solution. Taken together, these results highlighted the presence of planes characteristic of a zircon-type structure, which was consistent with the results determined by PXRD. Finally, X-EDS mapping (**Figure 11.c**) corroborated these findings. It confirmed the homogeneous distribution of zirconium, uranium, and silicon within the spherical particles and ruled out any elemental segregation during precipitation then purification. Moreover, no local heterogeneity likely to reveal traces of oxide or amorphous silica was detected. Thus, the purified chernobylite solid solution samples have been neither chemically nor morphologically altered compared to the raw materials after the three stages of selective dissolution. Additional scanning electron microscopy (SEM) observations were performed on the purified $Zr_{0.4}U_{0.6}SiO_4$ sample (initially prepared at a pH of 2.7, i.e. in the presence of large content of oxide as secondary phase). The images presented in **Figure SI.8.b** confirm that a pure phase was obtained after purification.

View Article Online
DOI: 10.1039/D6DT01220E

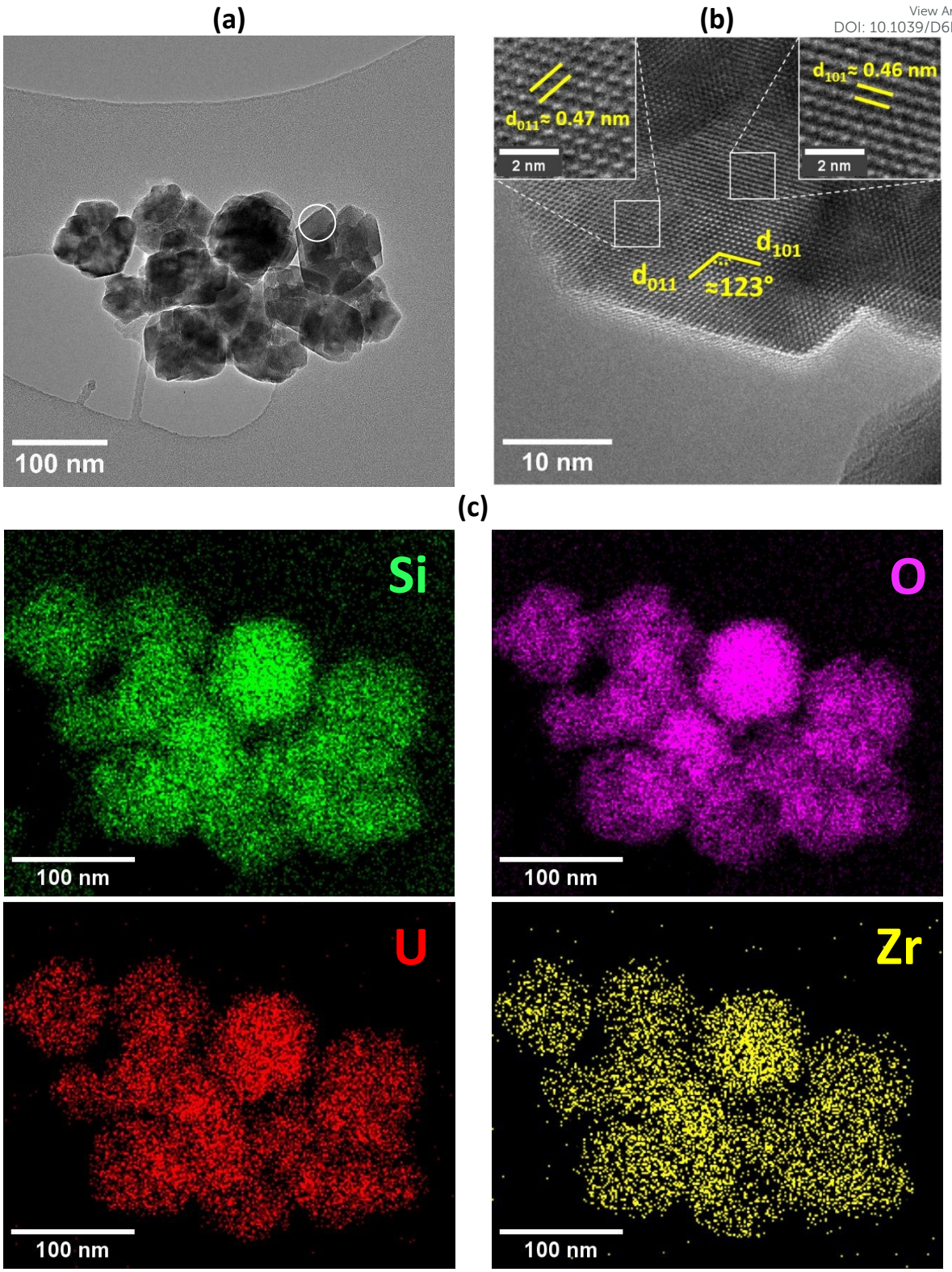

Figure 11. (a) TEM micrograph, (b) high-resolution TEM micrograph and (c) STEM-EDS analysis with the corresponding elemental maps of Si, O, Ti, and Zr, showing the elemental distribution of purified $Zr_{0.35}U_{0.65}SiO_4$ solid solution, showing the absence of oxide nanoparticles in the purified samples (sample 27). The white circle on **Figure 11.a** correspond to the spot selected for nano diffraction image reported in **Figure SI.4**.

In order to confirm the average particle size in the chernobylite solid solutions, specific surface area (S_{SA}) was measured using the BET method for both the raw and purified samples. The results are summarized in **Table 7**. For raw samples, S_{SA} values ranged from 19 ± 1 to 22 ± 1 $m^2 \cdot g^{-1}$, regardless of the composition. Such high S_{SA} values of the prepared samples reflected the presence of rather high porosity in the samples. After purification, these values were not significantly modified, except for the $Zr_{0.4}U_{0.6}SiO_4$ sample, for which S_{SA} decreased from 22 ± 1 $m^2 \cdot g^{-1}$ to 14 ± 1 $m^2 \cdot g^{-1}$. For this latter, such decrease was clearly associated with the elimination after purification of nanometric oxide and silica present in the raw sample, as demonstrated by PXRD. Assuming spherical particles, the average particle diameter calculated from **Eq. 1** and **Eq. 2** (see section 2.5.6) was between 40 nm ($Zr_{0.4}U_{0.6}SiO_4$) and 50 nm ($Zr_{0.6}U_{0.4}SiO_4$). Theses value were significantly lower than that observed for spherical agglomerates (approximatively 300 nm) but was in line with the size of the single crystals observed by TEM (approximatively 35 nm). Consequently, the agglomerates appeared to be highly porous. To verify the cohesion of solid solution agglomerates of chernobylite solid solution samples, ultrasonic treatments were also carried out for 30 seconds at 30 kHz. This led to the disintegration of the agglomerates into crystallites of approximatively 100 nm in length, reflecting the fragile nature of these agglomerates and confirming significant internal porosity (**Figure SI.8**).

Table 7. Results of BET analyses on raw and purified samples of $Zr_{1-x}U_xSiO_4$ (with x = 0.40, 0.50 and 0.60).

Composition	Phase	Specific area ($m^2 \cdot g^{-1}$)
$Zr_{0.60}U_{0.40}SiO_4$	Raw	21 ± 1
	Purified	22 ± 1
$Zr_{0.50}U_{0.50}SiO_4$	Raw	19 ± 1
	Purified	20 ± 1
$Zr_{0.40}U_{0.60}SiO_4$	Raw	22 ± 1
	Purified	14 ± 1

View Article Online
DOI: 10.1039/D6DT01220E

3.4. Thermal stability of chernobylite solid solutions

The chernobylite solid solution samples were successfully purified and examined for thermal stability by calcination at temperatures ranging from 1000 to 1300°C. Five compositions (x = 0.05, 0.20, 0.30, 0.50, and 0.60) were particularly studied. The results are presented in **Figure 12** for $Zr_{0.95}U_{0.05}SiO_4$, $Zr_{0.7}U_{0.3}SiO_4$ and $Zr_{0.4}U_{0.6}SiO_4$ solid solutions and in **Figure SI.11** for $Zr_{0.8}U_{0.2}SiO_4$ and $Zr_{0.5}U_{0.5}SiO_4$ solid solutions. Unit cell parameters of all these solid solutions were refined using the Le Bail method at different calcination temperatures (**Table SI.12**). These results indicate that the composition of the silicate phase did not vary significantly between 1000 and 1300°C regardless of the solid solution. For instance, the estimated uranium content in the silicate phase was equal to 3 mol.% for $Zr_{0.95}U_{0.05}SiO_4$, across the entire studied temperature. Similarly, uranium contents of approximately 21, 30 and 46 mol.% were determined for $Zr_{0.8}U_{0.2}SiO_4$, $Zr_{0.7}U_{0.3}SiO_4$, and $Zr_{0.5}U_{0.5}SiO_4$, respectively. Under these conditions, increasing the calcination temperature did not alter significantly the composition of the silicate phase. The $Zr_{0.95}U_{0.05}SiO_4$ solid solution appeared stable up to 1300°C (**Figure 12.a**). This observation was not surprising, as its composition was similar to that of zircon. Zircon itself is known to be stable up to approximately 1675–1700°C, according to Kaiser *et al*.[40] As observed for $Zr_{0.95}U_{0.05}SiO_4$, the $Zr_{0.7}U_{0.3}SiO_4$ solid solution appears to be generally stable across the entire temperature range studied. No decomposition or formation of secondary phases was detected within the analytical detection limits. In contrast, the $Zr_{0.5}U_{0.5}SiO_4$ solid solution (**Figure SI.11.b**) shows signs of decomposition at the highest temperatures. Indeed, an oxide phase appears, and its mass fraction increases from 10 ± 5 at 1200°C to 17 ± 5 wt.% at 1300 °C. Similarly, the $Zr_{0.4}U_{0.6}SiO_4$ solid solution exhibits signs of decomposition at 1300 °C, with an estimated oxide mass fraction of 13 ± 5 wt.%. These observations suggest that an increase in uranium content slightly destabilizes the silicate structure in favor of a mixture that includes mixed oxide phase and surely silica. However, the partial persistence of the silicate phase at high uranium content could indicate entropic stabilization due to the mixture of U and Zr combined with non-ideal mixing enthalpy effects. An ongoing calorimetric study should provide clearer answers in the future. [41]

View Article Online
DOI: 10.1039/D6DT01220E

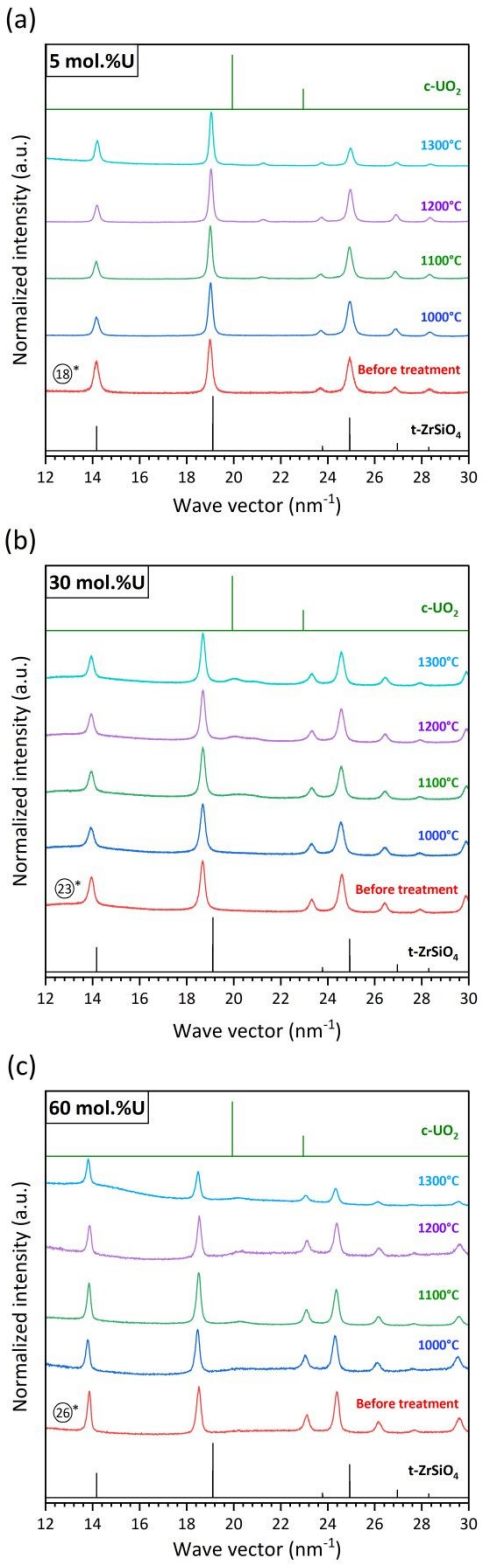

Figure 12. PXRD patterns recorded for (a) $Zr_{0.95}U_{0.05}SiO_4$, (b) $Zr_{0.7}U_{0.3}SiO_4$ and (c) $Zr_{0.4}U_{0.6}SiO_4$ chernobylite solid solutions after heating between 1000 and 1300°C under reducing atmosphere (Ar/4% H_2) during 6 hours. (18)*, (23)* and (26)* refer to purified (18), (23) and (26) chernobylite solid solution. All the samples were analyzed using laboratory XRD device (λ = 1.5418 Å). Reference data for tetragonal zircon (t-$ZrSiO_4$) and cubic UO_2 (c-UO_2) are taken from [30] and [31] respectively.

View Article Online
DOI: 10.1039/D6DT01220E

4. Conclusion

The synthesis of chernobylite solid solution developed in this study enabled optimization of experimental parameters that promote uranium incorporation into the zircon structure. A pH value of 1.6 and a hydrothermal treatment time of 7 days at 250°C appeared to significantly reduce the amount of oxide in the polyphase system. Under these conditions, uranium (IV) hydrolysis was limited while zirconium and uranium (IV) precipitated quantitatively as silicate compounds. These conditions were also essential for forming a homogeneous $Zr_{1-x}U_xSiO_4$ solid solution, limiting uranium (IV) oxidation to uranyl and inhibiting secondary phase formation (amorphous silica and nanometric oxide).

The uranium enriched samples, obtained at the end of the optimized hydrothermal treatment, were found to be polyphasic, requiring the development of a purification protocol. Alternating between basic, acidic, and then basic washing steps effectively eliminated amorphous silica and nanometric oxide. Conversely, no significant alteration of the silicate phase was observed.

Under these conditions, purified chernobylite solid solution samples with a wide range of compositions ($x \leq 0.6$) were successfully prepared. The uranium incorporation achieved was significantly higher than that observed in natural zircon specimens (approximately 12 mol.%) or samples prepared by dry chemistry routes (approximately 5 mol.%). Although unusual behavior was observed for low uranium contents ($x \leq 0.2$), possibly reflecting a different uranium incorporation mechanism, the solid solutions generally follow a Retger's law, indicating near ideal solid solution up to $Zr_{0.4}U_{0.6}SiO_4$. However, complete uranium substitution was not achieved, which is consistent with the instability of coffinite, $USiO_4$, under these synthesis conditions. Therefore, the development of phases richer in uranium now requires considering alternative synthesis route inspired by coffinite formation.

Finally, we studied the thermal stability of the purified chernobylite solid solution between 1000°C and 1300°C. Regardless of the composition of the solid solutions studied ($Zr_{0.95}U_{0.05}SiO_4$, $Zr_{0.8}U_{0.2}SiO_4$, $Zr_{0.7}U_{0.3}SiO_4$, $Zr_{0.5}U_{0.5}SiO_4$, and $Zr_{0.4}U_{0.6}SiO_4$), no significant decomposition was observed. This behavior suggests that these materials were thermally stable across the entire investigated composition range, despite slight decomposition of the samples at 50 and 60 mol % U at the highest temperatures. Thermodynamic analyses of the samples using drop calorimetry are underway to confirm these findings.

View Article Online
DOI: 10.1039/D6DT01220E

Authors Credits

Arthur Avallone: Writing – review & editing, Writing – original draft, Visualization, Methodology, Investigation, Formal analysis, Data curation, Conceptualization. **Léna Carette:** Writing – original draft, Data curation, Investigation, Formal analysis. **Paul Estevenon:** Writing – review & editing, Writing – original draft, Visualization, Validation, Methodology, Formal analysis, Data curation, Investigation, Conceptualization, Supervision. **Pascal G. Yot:** Writing – review & editing, Writing – original draft, Validation, Formal analysis, Data curation, Methodology. **Christoph Hennig:** Writing – review & editing, Data curation, Formal analysis. **Eleanor Lawrence Bright:** Writing – review & editing, Data curation, Formal analysis. **Renaud Podor:** Writing – review & editing, Data curation, Formal analysis, Investigation. **Xavier Le Goff:** Writing – review & editing, Data curation, Formal analysis, Investigation. **Pâmella Vasconcelos Borges Pinho:** Writing – review & editing. **Nicolas Clavier:** Writing – review & editing, Writing – original draft, Visualization, Supervision. **Xiaofeng Guo:** Writing – review & editing. **Christine Guéneau:** Writing – review & editing, Validation, Funding acquisition, Conceptualization, Project Administration, Supervision. **Nicolas Dacheux:** Writing – review & editing, Writing – original draft, Visualization, Validation, Methodology, Formal analysis, Data curation, Investigation, Funding acquisition, Conceptualization, Project Administration, Supervision.

Conflicts of interest

The authors declare no competing financial interest.

Acknowledgements

The authors acknowledge the European Synchrotron Radiation Facility for provision of synchrotron radiation facilities under proposal numbers A20-01-880 and CH-7418 (https://www.doi.org/10.15151/ESRF-ES-1671355592, https://www.doi.org/10.15151/ESRF-ES-2128052223, https://www.doi.org/10.15151/ESRF-ES-2128052287) and we would like to thank the ROBL team for assistance in using beamline BM20. The authors would also like to thank the following people for their assistance: Alban Jonchère and Lorenzo Callejon from ICSM for analyses of the Raman spectra, Laurent Claparede and Anthony Di Rinaldo from ICSM for performing the BET analyses, and Beatrice Baus-Lagarde from ICSM for assisting with the ICP-OES measurements. PhD work of Arthur Avallone has been funded by CEA and ASNR. The present study was also supported by the EPIC project funded by the French NEEDS (Nucléaire: Energie, Environnement, Déchets, Société) program (CNRS, CEA, ANDRA, BRGM, EDF, FRAMATOME, ASNR, ORANO). Xiaofeng Guo also acknowledge the support from the National Science Foundation, Division of Materials Research, award No. 2144792.

Declaration of Generative AI and AI-assisted technologies in the writing process

During the preparation of this work, the authors used DeepL for translation purposes and Chatgpt for the finalization of the graphical abstract. After using this tool/service, the authors reviewed and edited the content as needed and take full responsibility for the content of the published article.

Data availability

The data supporting this article have been included as part of the ESI.

View Article Online
DOI: 10.1039/D6DT01220E

Author information

Corresponding author

*N. D.: phone. +33 4 66 33 92 05; e-mail. nicolas.dacheux@umontpellier.fr

ORCiD

Arthur Avallone: 0009-0005-7005-2070
Léna Carette: 0009-0008-4455-0756
Paul Estevenon: 0000-0001-8517-4744
Pascal G. Yot: 0000-0003-1401-5708
Christoph Hennig: 0000-0001-6393-2778
Eleanor Lawrence Bright: 0000-0002-3659-6833
Renaud Podor: 0000-0002-8103-1743
Xavier Le Goff: 0000-0002-5041-0468
Pâmella Vasconcelos Borges Pinho: 0000-0001-7725-2124
Nicolas Clavier: 0000-0001-8010-2661
Xiaofeng Guo: 0000-0003-3129-493X
Christine Guéneau: 0000-0001-5207-9740
Nicolas Dacheux: 0000-0003-1636-1313

View Article Online
DOI: 10.1039/D6DT01220E

5. References

1 B. E. Burakov, E. B. Anderson, B. Ya. Galkin, E. M. Pazukhin and S. I. Shabalev, *Radiochimica Acta*, 1994, **65**, 199–202.

2 P. Pöml, B. Burakov, T. Geisler, C. T. Walker, M. L. Grange, A. A. Nemchin, J. Berndt, R. O. C. Fonseca, P. D. W. Bottomley and R. Hasnaoui, *Journal of Nuclear Materials*, 2013, **439**, 51–56.

3 V. V. Gurzhiy, B. E. Burakov, A. V. Kasatkin, Y. Yu. Petrov, V. A. Orlova and A. A. Agakhanov, *Journal of Nuclear Materials*, 2026, **618**, 156195.

4 S. V. Gabielkov, I. V. Zhyganiuk, V. G. Kudlai, B. S. Savchenko, P. E. Parkhomchuk and S. O. Chikolovets, *Journal of Nuclear Materials*, 2025, **614**, 155893.

5 E. B. Anderson, B. E. Burakov and E. M. Pazukhin, *Radiochimica Acta*, 1993, **60**, 149–152.

6 R. Finch and J. Hanchar, *Reviews in Mineralogy and Geochemistry*, 2003, **53**, 1–25.

7 J. A. Speer, *Reviews in Mineralogy and Geochemistry*, 1980, **5**, 113–135.

8 N. Nazir, R. Ayyamperumal, K. U. Majeed and C. Zhang, *Geological Journal*, 2022, **57**, 3463–3477.

9 W. J. Weber, R. C. Ewing and J. Lian, *J. Appl. Phys.*, 2004, **95**, 5949–5971.

10 Ceramic Waste Forms for Actinides | Elements | GeoScienceWorld, https://pubs.geoscienceworld.org/msa/elements/article-abstract/2/6/365/137726/Ceramic-Waste-Forms-for-Actinides, (accessed December 15, 2025).

11 Radiation effects in crystalline ceramics for the immobilization of high-level nuclear waste and plutonium | Journal of Materials Research | Cambridge Core, https://www.cambridge.org/core/journals/journal-of-materials-research/article/radiation-effects-in-crystalline-ceramics-for-the-immobilization-of-highlevel-nuclear-waste-and-plutonium/09D70E1FB1A625EC09BB98883C3A5ED3, (accessed December 15, 2025).

12 X. Guo, S. Szenknect, A. Mesbah, S. Labs, N. Clavier, C. Poinssot, S. V. Ushakov, H. Curtius, D. Bosbach, R. C. Ewing, P. C. Burns, N. Dacheux and A. Navrotsky, *Proceedings of the National Academy of Sciences*, 2015, **112**, 6551–6555.

13 J. Janeczek and R. C. Ewing, *MRS Proceedings*, 2011.

14 D. Langmuir, *Geochimica et Cosmochimica Acta*, 1978, **42**, 547–569.

15 S. Szenknect, D. Alby, M. López García, C. Wang, R. Podor, F. Miserque, A. Mesbah, L. Duro, L. Zetterström Evins, N. Dacheux, J. Bruno and R. C. Ewing, *Sci Rep*, 2020, **10**, 12168.

16 A. Mesbah, S. Szenknect, N. Clavier, J. Lozano-Rodriguez, C. Poinssot, C. Den Auwer, R. C. Ewing and N. Dacheux, *Inorg. Chem.*, 2015, **54**, 6687–6696.

17 R. Valero, Haute Alsace, 1997.

18 R. Valero, .

19 T. Barral, P. Estevenon, Y. Chanteau, T. Kaczmarek, A. C. Strzelecki, D. Menut, E. Welcomme, S. Szenknect, P. Moisy, X. Guo and N. Dacheux, *Dalton Trans.*, 2023, **52**, 10023–10037.

20 N. Dacheux, A. Avallone, P. Estevenon, C. Hennig, S. Szenknect, K. Kvashnina, P. Vasconcelos Borges de Pinho, N. Clavier, X. Guo and C. Guéneau, presented in part at the 2025 MRS Spring Meeting & Exhibit, Seattle, WA, September, 2025.

21 L. H. Fuchs and H. R. Hoekstra, *American Mineralogist*, 1959, **44**, 1057–1063.

22 S. Szenknect, A. Mesbah, T. Cordara, N. Clavier, H.-P. Brau, X. Le Goff, C. Poinssot, R. C. Ewing and N. Dacheux, *Geochimica et Cosmochimica Acta*, 2016, **181**, 36–53.

23 N. Clavier, S. Szenknect, D. T. Costin, A. Mesbah, J. Ravaux, C. Poinssot and N. Dacheux, *Journal of Nuclear Materials*, 2013, **441**, 73–83.

24 P. Estevenon, Université de Montpellier, 2018.

25 P. Estevenon, T. Barral, A. Avallone, M. Jeffredo, A. De La Hos, A. Strzelecki, X. Le Goff, S. Szenknect, K. Kvashnina, P. Moisy, R. Podor, X. Guo and N. Dacheux, *Dalton Trans.*, 2024, **53**, 13782–13794.

View Article Online
DOI: 10.1039/D6DT01220E

26 N. Dacheux, V. Brandel and M. Genet, *New Journal of Chemistry*, 1995, **19**, 1029–1036.
27 A. P. Hammersley, S. O. Svensson, M. Hanfland, A. N. Fitch and D. Hausermann, *High Pressure Research*, 1996, **14**, 235–248.
28 A. Boultif and D. Louër, *J Appl Cryst*, 1991, **24**, 987–993.
29 V. Petříček, M. Dušek and L. Palatinus, *Zeitschrift für Kristallographie - Crystalline Materials*, 2014, **229**, 345–352.
30 F. J. Torres, M. A. Tena and J. Alarcón, *Journal of the European Ceramic Society*, 2002, **22**, 1991–1994.
31 G. Leinders, T. Cardinaels, K. Binnemans and M. Verwerft, *Journal of Nuclear Materials*, 2015, **459**, 135–142.
32 V. Neck and J. I. Kim, *Radiochimica Acta*, 2001, **89**, 1–16.
33 L. Callejon, M. Fulchiron, L. Claparede, J. Lautru, N. Clavier, R. Podor, S. Szenknect and N. Dacheux, *Journal of the European Ceramic Society*, 2025, **45**, 117710.
34 L. Claparede, F. Tocino, S. Szenknect, A. Mesbah, N. Clavier, P. Moisy and N. Dacheux, *Journal of Nuclear Materials*, 2015, **457**, 304–316.
35 K. Breiter, H.-J. Förster and R. Škoda, *Lithos*, 2006, **88**, 15–34.
36 E. V. Shalaeva, A. M. Murzakaev, V. V. Makarov, V. G. Pushin, D. A. Zamyatin, Yu. V. Shchapova and S. L. Votyakov, *Glass Phys Chem*, 2015, **41**, 389–397.
37 S. V. Ushakov, W. Gong, M. M. Yagovkina, K. B. Helean, W. Lutze and R. C. Ewing, *Ceram. Trans.*
38 P. Estevenon, T. Kaczmarek, F. Vadot, T. Dumas, P. L. Solari, E. Welcomme, S. Szenknect, A. Mesbah, P. Moisy, C. Poinssot and N. Dacheux, *Dalton Trans.*, 2019, **48**, 10455–10463.
39 A. C. Strzelecki, T. Barral, P. Estevenon, A. Mesbah, V. Goncharov, J. Baker, J. Bai, N. Clavier, S. Szenknect, A. Migdisov, H. Xu, R. C. Ewing, N. Dacheux and X. Guo, *Inorg. Chem.*, 2021, **60**, 718–735.
40 A. Kaiser, M. Lobert and R. Telle, *Journal of the European Ceramic Society*, 2008, **28**, 2199–2211.
41 J. Marcial, Y. Zhang, X. Zhao, H. Xu, A. Mesbah, E. T. Nienhuis, S. Szenknect, J. C. Neuefeind, J. Lin, L. Qi, A. A. Migdisov, R. C. Ewing, N. Dacheux, J. S. McCloy and X. Guo, *npj Mater Degrad*, 2021, **5**, 34.

View Article Online
DOI: 10.1039/D6DT01220E

Revisiting Synthesis of Pure chernobylite Solid Solutions for Thermal Stability Investigations

Arthur Avallone [1], Léna Carette [1], Paul Estevenon [2], Pascal G. Yot [3], Christoph Hennig [4, 5], Eleanor Lawrence Bright [4, 5], Renaud Podor [1], Xavier Le Goff [1], Pâmella V. B. Pinho [6], Nicolas Clavier [1], Xiaofeng Guo [7, 8], Christine Guéneau [6], Nicolas Dacheux [1, *]

1 ICSM, Univ Montpellier, CNRS, CEA, ENSCM, Bagnols-sur-Cèze, France

2 CEA, DES, ISEC, DMRC, Univ Montpellier, Marcoule, France

3 ICGM, Univ Montpellier, CNRS, ENSCM, Montpellier, France

4 Institute of Resource Ecology, Helmholtz Zentrum Dresden-Rossendorf (HZDR), PO Box 510119, 01314 Dresden, Germany

5 The Rossendorf Beamline at ESRF, The European Synchrotron, CS40220, 38043 Grenoble Cedex 9, France

6 Université Paris-Saclay, CEA, Service de recherche en Corrosion et Comportement des Matériaux, Gif-sur-Yvette, France

7 Department of Chemistry, Washington State University, Pullman, Washington 99164, United States

8 Alexandra Navrotsky Institute for Experimental Thermodynamics, Washington State University, Pullman, Washington 99164, United States

* Corresponding of author: nicolas.dacheux@umontpellier.fr

View Article Online
DOI: 10.1039/D6DT01220E

Data statement

The data supporting this article have been included as part of the ESI.